Surface Modification of High-Temperature Alloys: A Protective and Adhesive Scale-Forming Process*

J.-H. Park[+] and W. D. Cho[++]

[+]Energy Technology Division, Argonne National Laboratory, Argonne, Illinois 60439

[++]Department of Metallurgical Engineering, University of Utah, Salt Lake City, Utah 84112

July 1995

INVITED paper for presentation at 4th International Symposium on Processing and Fabrication of Advanced Materials IV, Cleveland, Ohio, Oct. 30-Nov. 2, 1995.

*This work has been supported by the U.S. Department of Energy, under Contract W-31-109-Eng-38.

Surface Modification of High-Temperature Alloys: A Protective and Adhesive Scale-Forming Process*

J.-H. Park[+] and W. D. Cho[++]

[+]Energy Technology Division, Argonne National Laboratory, Argonne, Illinois 60439
[++]Department of Metallurgical Engineering, University of Utah, Salt Lake City, Utah 84112

ABSTRACT

To develop a high-quality protective/adhesive scale-forming surface modification technique, several stepwise experiments were performed on the alloys of Fe-25Cr, Fe-25Cr-(0.3-1)Y, and Fe-25Cr-(0.3-1)Ce: alloy grain-growth behavior, surface coatings by ion-beam-assisted deposition (IBAD) and high-temperature chemical vapor deposition (CVD), and oxidation/sulfidation tests. Silicon-based oxide, nitride, and oxinitride coatings were prepared by IBAD. During annealing, the silicon diffuses into and reacts with the substrate to form a metal-silicide. To verify the scale-forming mechanism, oxidation tests (at temperatures of 700-1000°C and oxygen partial pressure of 10^{-4} atm) were performed on substrates with and without the coating layer. The results showed that Cr_2O_3 was formed as the outer scale and that a thin SiO_2 layer

*This work has been supported by the U.S. Department of Energy, under Contract W-31-109-Eng-38.

was observed at the alloy/scale interface. Based on these results, an alternative surface-modification approach was tried. A durable protective coating for high-temperature alloys was achieved by CVD followed by chemical reaction in a controlled environment. By thermogravimetric analysis with a microbalance, several oxidation/sulfidation tests (at 700 and 1000°C) were performed with and without the coating on Fe-25Cr-1Ce and Fe-25Cr-1Y. After each run, samples were examined by scanning electron microscopy, energy-dispersive X-ray analysis, and Auger and X-ray photoelectron spectroscopy. The results elucidated the nature of the protective coating that provides high-temperature corrosion protection.

INTRODUCTION

Corrosion resistance of structural alloys in high-temperature environments is typically achieved by the formation of a continuous chromium oxide (Cr_2O_3) scale. This scale acts as a rate-determining solid-state diffusion barrier between the environment and alloy substrates. Two fundamental aspects of high-temperature oxidation studies are the elucidation of transport mechanisms to reduce oxidation kinetics, and improvement of scale adhesion to the alloy substrate. This study has focused on several issues to fabricate improved protective scales for use in high-temperature corrosive environments.

Protective Scale Formation

In 1937, Pfeil[1] discovered that trace additions of oxygen-active elements such as Y, La, and Ce to alloys that form chromium or aluminum oxide scales upon exposure to high temperatures have a highly beneficial effect on the oxidation behavior of alloys. Specially in the case of chromia formers, it was found that addition of the so-called "reactive-elements" reduces the growth rate of the oxide layer and enhances the adhesion of the oxide to the base alloy, whereas in the case of alumina formers, the growth rate is not affected. This effect is known as the "reactive-element effect (REE)." Recently, substantial progress has been made in explaining the mechanisms of this effect. Reports of recent investigations on the reactive elements and on the transport properties of the oxide materials are available in the literature, [2-4] as is a detailed description of basic mechanisms of high-temperature corrosion.[5]

Initial Stage of Scale Forming Process

The nature of the nucleation sites has always been a great interest. Many investigators[5] have proposed that nucleation is favored at sites of higher energy, i.e., at surface defects in the form of dislocations, grain boundaries, impurities, etc. Some have concluded that homogeneous nucleation takes place in the adsorbed layer. It appears that the particular predominant mechanism is dependent on the metal and the pretreatment of its surface, temperature, and oxygen pressure (e.g., the degree of supersaturation in the adsorbed layer). However, at weak supersaturation and relatively high temperatures, defects in the adsorption layer may be annealed out, and only defects in the metal surface remain in appreciable numbers.[6] Thus, at high supersaturation the number of nuclei can greatly exceed the number of dislocations. Under these conditions, homogeneous nucleation probably predominates and would qualitatively explain the large influence of oxygen pressure on the density of oxide nuclei at relatively high temperatures (nuclei density is also a function of the metal surfaces). These differences can be related to epitaxial relationships between the oxide nuclei and the metal substrate. It should be emphasized that the substrate surface must be clean, because the presence of impurities can change or completely inhibit the epitaxial relationships. The characteristics of initial-stage oxidation, (M + O = MO) could be directly related to the initial process for simulating the protective coating development, as in a high temperature chemical vapor deposition (CVD) process.[7]

Diffusion Model Approach

One of the most common protective oxide scales for high-temperature corrosion is chromia which is known to grow via outward diffusion of cations from the metal to the oxide/gas interface. A Wagnerian model could be the

most fundamental approach in high-temperature corrosion of alloys and in any diffusion-related process based on point defects. However, bulk diffusion of cations, as measured in chromia single crystals, is orders of magnitude too slow to explain the observed rates of oxidation in alloys that form chromia scales. Graham et al. proposed from the results of SIMS studies for Cr oxidation that cation diffusion along or through high-diffusivity paths controls chromia forming-oxidation.[8] A detailed approach for a diffusion model that could be applicable to practical systems was established by Whipple[9] in 1965, followed by Suzuoka[10] and Le Claire[11] in the 1970s. They were attempting to determine the grain-boundary and subboundary diffusion profile, along with bulk diffusion. The model established for grain-boundary diffusion was based on an empirical data treatment to make a best fit to the linear relationship between concentrations of diffusing species with depth. In the 1980s, Atkinson and Taylor[12] attempted to find a correlation between the rates of oxidation of nickel and partial pressure of oxygen (pO_2) dependence of diffusion; they obtained almost ideal results that fit well with both oxidation rates and diffusion measurements in independent approaches. Park et al.[13] measured the bulk, subboundary, and grain-boundary diffusivities on sintered Cr_2O_3 at 1100°C and in a pO_2 that corresponds to Cr/Cr_2O_3 equilibrium to find the oxidation mechanism of pure and Y-doped chromium. The result indicated that the oxidation rate was at least 10 times higher than that of the calculation using diffusion data (from the sum of the contributions of bulk, subboundary, and grain-boundary). According to the data for oxidation rates reported by Lileurud and Kofstad,[14] the data were 10-10,000 times higher than those calculated from the diffusion data. The calculated oxidation rate using diffusion data was the lowest among the reported oxidation rates for chromia-forming

oxidation.[13] It is obvious that there may be some other faster diffusion path(s) that could be wide-open grain boundaries due to growth stresses and deformation of scales. Grain-boundary sliding proposed by Evans and Langdon[15] could be one of the most important scale-forming processes: A high-temperature process could be related to surface diffusion which is expected to be the main diffusion process during high-temperature corrosion. Therefore, this might be one of the important open questions in correlating diffusion measurements with microstructures of growing scales. Previous work[16] showed that reactive elements inhibit grain growth in the alloy and pure Cr during oxidation, and suppress Fe diffusion through the scale in Fe-Cr alloys.

Reactive-elements effect: In the alloy or in the scale ?

We must determine whether the reactive elements-effect (REE) occurs within the alloy or within the scale, based on the fundamental mechanism of the REE on enhanced adhesion between an oxide scale and the alloy substrate. An attempt was made by comparing reaction bonding at the interfaces of Cr/Cr_2O_3 couples in which yttrium was initially present on the Cr side vs. the Cr_2O_3 side and both sides. From these observations, we concluded that the trace addition of yttrium on the alloy side gives rise to enhanced adhesion between the oxide scale and the base alloy during high temperature oxidation.[17] It may be necessary to find the relationship between the enhanced adhesion and rates of oxidation. However, when the enhanced-adhesion effect is relevant during oxidation, we must consider the roles of reactive elements in the alloy or in the scale because the diffusion approach indicates that the presence of yttrium gives rise to higher diffusivities of both oxygen and

chromium in sintered Cr_2O_3 at 1100°C and in a pO_2 that corresponds to Cr/Cr_2O_3 equilibrium.[13,18] This trend suggests that the REE for the Y case does not occur in the scale, but its role could be important in the alloy substrate during high-temperature processes.

Stabilization of alloy substrate

Because the REE is important in high-temperature processing of alloys, it is necessary to see the effect of reactive elements on the stabilization of alloys. Such alloy stabilization could be observed in alloys containing reactive elements.[16] This trend has a doubly beneficial effect on the scale-forming process. Reactive elements tend to inhibit grain growth, i.e., they stabilize the alloy substrate during high-temperature oxidation. Rapp[19] has pointed out that grain growth in the metal substrate during scaling could locally destroy the initial metal/scale epitaxial relationships and thereby lead to debonding of the interface. For this reason, the poor adherence of scale formed by cation diffusion, especially for cyclic oxidation, is understandable. Oxidation testing indicated that the scale formed by the oxidation of Fe-25Cr (no addition of reactive elements) at 1000°C was totally spalled after the samples were cooled. However, the scales in Y-containing alloys (Fe-25Cr-0.3Y and 1Y) were not spalled, and alloy grains were not growing under the same oxidation conditions used for Fe-25Cr.[16] We therefore conclude that reactive elements stabilize substrates during high-temperature processing.[20] King et al.[21] investigated the scale/alloy interface of Fe-25Cr-0.87Y alloy: Y_2Fe_{17}, with a hexagonal structure, was a stable grain-boundary compound, and $Y_2(Fe, Cr)_{17}$ was identified at the alloy grain boundary; consequently, $Y_2(Fe, Cr)_{17}$ stabilizes the alloy substrate and acts as a grain-growth inhibitor[20] in the alloy (Fig. 1). To

prove that alloy stabilization is important, pre-enlarged grains by high-temperature annealing of Fe-25Cr samples were oxidized and cooled. No spallation was observed after thermal quenching of the pre-enlarged grain samples of Fe-25Cr.[20]

Preferential Diffusion Species via Scale

Generally, inward anion diffusion is expected to give better adhesion because the scale forms near the scale/alloy interface by the chemical reaction between metal cations and oxygen anions: $M^{+2} + O^{-2} = MO$. For high-temperature oxidation of the Y-containing alloy, it has been verified that the anion undergoes inward diffusion.[22] If cation outward diffusion is predominant, the alloy/scale interface may not be stable during that process, but when the anions are moving inward and react with the alloy, the bonding process could be spontaneous at the scale/alloy interface.

Remaining issues to improve corrosion resistance

Thus far, we have discussed the behavior of reactive elements during high-temperature corrosion by considering several important aspects. Finding improved materials for corrosion inhibition and fabricating materials of high corrosion resistance are the tasks we now face. However, to test various bulk-composition alloys with screening-type experiments requires much effort because altering the alloy compositions is normally used to determine material properties (mechanical, chemical, thermal, etc.). It is obvious that proper heat treatment in correctly designed environments, or simply surface modifications on ready-made materials, may be feasible methods for improving the corrosion resistance of alloys.

Because corrosion problems occur mainly at the surface and alloy/scale interfaces, finding a method for stable surface modification of high-temperature alloys is one of the most important issues. We may consider the initial stages of alloy corrosion and high-temperature CVD as similar processes because in both cases, gases react with and diffuse into the alloy substrate. The initial corrosion process could be considered as a spontaneous reaction occurring between cations from the alloy and anions from the environment. Many dopants can be added to the bulk alloy to reduce the oxidation rate by reducing atomic diffusion. These attempts are based on scale-defect chemistry and the microstructure developed during the process. In modifying an alloy by coating, we must consider both thermodynamic and kinetic stability with respect to the environment in order to create an ideal passivation layer and compatibility with the alloy substrate. However, the coating procedure also involves other concerns similar to those discussed above. Thermal expansion coefficients, and the alloy surface microstructure (here, the definition of surface depends on temperature: high-temperature surfaces are deeper than those at low temperature, based on the temperature dependence of diffusivity). The surface contains (a) a crystallographically perfect layer, but with various orientations, equilibrium point defects (intrinsic) and impurity-related point defects (extrinsic), and surface-terminated dislocations are present in the grain (b) grain boundaries of different angles; and (c) open-void, wide-open grain boundaries, and microcracks and fissures, as shown in Ref. 2.

The objective of the this study is to develop an effective surface modification for corrosion protection of high-temperature alloys beyond that achieved by reactive-element additions (such as Fe-25Cr-1Y). Several experimental steps were conducted to determine the highest degree of

protection available in high-temperature gaseous environments containing oxygen and sulfur.

EXPERIMENTAL PROCEDURES

To fabricate a silicon-oxygen-nitrogen (Si-N-O) coating layer, (a) an ion-beam-assisted-deposition (IBAD) technique, which is generally accepted as producing the most dense coating for low-temperature surface modification with Fe-25Cr- 1Y, and (b) high-temperature CVD for Fe-25Cr-1Y and Fe-25Cr-1Ce was used. Experiments were conducted in several steps for the alloys with and without REE samples: (a) oxidation and sulfidation tests, (b) alloy grain growth observations, and (c) oxidation/sulfidation tests for the surface-modified alloys of Fe-25Cr-(0.3 and 1)Y by IBAD and CVD.

Alloy grain growth: To investigate alloy grain-growth behavior with and without REE, bearing samples of Fe-25Cr, Fe-25Cr-1Y, and Fe-25Cr-1Ce were examined after exposure at 1000°C for periods of 44 min, 2 h 52 min, 8 h 20 min, and 24 h 40 min. Alloy samples were wrapped with tantalum metal sheet and placed in quartz tubes having one closed end and vacuum sealed off. Microstructures were examined by optical microscopy; some were also examined by scanning electron microscopy and for chemical analysis of the surface by EDS. Figure 2 shows grain-growth behavior of the Fe-25Cr alloys with and without REE. After the 40-min annealing, the Fe-25Cr alloy grains were about 10 times larger than their original size, but the grain size of the Y- and Ce-containing alloys remained the same or grew by < 5%. The Fe-25Cr-1Y grains grew < 1% during 25 h. Figure 3 shows the detailed surface of the (a) Fe-25Cr, (b) Fe-25Cr-1Y, and (c) Fe-25Cr-1Ce, respectively. As seen in Figs. 2

and 3, Fe-25Cr-1Ce alloy showed a somewhat different grain growth behavior. Cerium segregation onto the alloy surface was observed: after the 8-h annealing, very fine particles were distributed homogeneously over the alloy surface, while after 25 h, the cerium particles grew larger and appeared to coagulate but without local preference, i.e., grain-boundary segregation behavior was not predominant.

Surface Coatings and Oxidation and Sulfidation Tests:

Ion Beam Assisted Deposition. For the IBAD process, a nitrogen ion beam of 500 eV and 1 mA was applied on the Fe-25Cr-1Y surface to produce a coating thickness of 1.5 μm. A schematic drawing of the apparatus is shown in Fig. 4. Figure 5 shows the surface and a cross section of the Si-N coating. As seen in the cross section, adhesion between the coating and base alloy substrate is good; however, the X-ray diffraction pattern does not show any detectable signals due to the amorphous state (Table 1). When the samples were heated at 500°C for 2 h in argon, the surface became Fe-Cr-silicide and Cr_2O_3 according to X-ray diffraction; Auger and X-ray photoelectron spectroscopy show the main composition at the surface to be Si, N, and O. The heat treated samples were not visually different, except at the very edge where a minor spallation was observed. The coated samples were subjected to oxidation (700-1000°C) in flowing N_2-O_2 ($pO_2 = 10^{-4}$ atm).

High-Temperature CVD: Coatings on high-temperature alloys were produced by CVD with a mixture of NaF-Si-SiO_2 used as a source of silicon vapor to produce a 1.5-μm-thick coating on Fe-25Cr-1Y and Fe-25Cr-1Ce surfaces. This was followed by an annealing to diffuse the silicon into the bulk

alloy, and exposure to ammonium vapor to form a silicon/oxygen/nitrogen phase at the surface by chemical reaction. A schematic drawing of the apparatus is shown in Fig. 6. In Fig. 7, weight gain versus sample position is shown, while the CVD samples of Fe-25Cr-1Y and Fe-25Cr-1Ce are shown, along with EDS analysis, in Figs. 8 and 9. Figure 9a shows silicon diffusion (the darker gray areas) into and around surface defects, fissures, and microcracks that are normally the chemically active sites where corrosion begins on the surface of the alloy, and Fig. 9(b) is an enlargement of the area at the right-center of Fig. 9a. In the TEM sample (Fig. 10), we find silicon diffusion around alloy grain boundaries, which are also normally the chemically active sites where corrosion begins on the surface of the alloy.

To compare corrosion behavior of coated and uncoated samples, several oxidation and sulfidation tests were performed at 700-1000°C in a thermogravimetric microbalance. After each run, samples were examined by scanning electron microscopy and by EDS and Auger and X-ray photo-electron spectroscopy.

RESULTS AND DISCUSSION

Alloy grain growth observation: The use of cerium as a REE is somewhat of a dilemma because phase melting is expected during high-temperature processes.[23,24] Yttrium-containing alloys are very stable even during extended treatment times (25 h), but undoped Fe-25Cr shows some compositional separation within the enlarged grains. However, this grain-growth behavior in high-temperature alloys is of concern in regard to maintaining adhesion during oxidation or the coating process. As Rapp,[19] Park and Natesan,[20] and Shore[25]

have pointed out, grain growth in the metal substrate during scaling could locally or even totally destroy the initial metal/scale epitaxial relationships and thereby lead to debonding of the interface. For these reasons, the poor adherence of cation-diffusing scales (especially for cyclic oxidation) is understandable. Hillert[26] proposed the final fractional size of second-phase particles versus alloy grain size in the base alloy for the inhibition in the alloy grain growth: for the low fraction of second phase, $D/r = 3.6/f^{0.333}$, where D is the average grain size, r is the particle radius and f the volume fraction of the second phase, and grain growth will end when the relationship of $D/r = 0.89/f^{0.889}$ is reached. In the present study, yttrium-containing particles in the alloy are 0.2-0.3 μm in size, depending on the amount we put into the alloy, and the alloy grains do not grow after fabrication. This trend for yttrium-containing alloys fits well into the model proposed by Hillert.[26]

Surface coatings on alloy samples: The results of alloy grain growth behavior at high-temperatures will allow us to choose proper alloys for further experiments of surface modification in order to study high-temperature oxidation.

Ion-Beam-Assisted Deposition (IBAD). Figure 11 shows a cross section of the surface-modified alloy (Fe-25Cr-0.3Y/Si-N-O) after oxidation in a N_2/O_2 gas mixture at 900°C for 69 h. Adhesion at the scale/alloy interface is good; the scale/alloy interface is wavy along the boundary but the gas/scale interface appears flat. By comparing scale thicknesses, we could expect that the parabolic oxidation rates are similar for the surfaces with and without coating. From analysis of the cross section of an oxidized sample, the highest concentration of silicon is near the scale/alloy interface (Fig. 12). In the depth

profile (Fig. 13), silicon is spread throughout the scale but is more concentrated near the interface.

High-temperature chemical vapor deposition (CVD). Surface modification via CVD improves the protective properties of alloys when they are exposed to corrosive gases and/or oxygen at high temperatures. Without the benefit of an effective and long–lasting protective coating, the alloys are attacked initially at microscopic surface defects, fissures, and micro-cracks, which are chemically active sites.

Oxidation. Figure 14 shows weight change versus time of oxidation of Fe-25Cr-1Ce, Fe-25Cr-1Y, and Fe-25Cr-0.3Y/CVD alloys in air at 1000°C. Figure 15 shows the oxidized surface of Cr_2O_3 for Fe-25Cr-0.3Y/CVD alloy. Locally, several oriented chromia crystals were found after 55 days exposure at 1000°C in air. These Cr_2O_3 crystals provide evidence of local Cr outward diffusion during oxidation. The parabolic rate constant (k_g) calculated from Fig. 14, i.e., for 30 days, is 3.86×10^{-13} $g^2/cm^4 \cdot s$ (or, $\log k_g = -12.41$ $g^2/cm^4 \cdot s$). Assuming a Cr_2O_3 scale with theoretical density, $\rho_{ox} = 5.225$ g/cm^3 and the average weight fraction of oxygen in the oxide, $h = 48/152$, then we calculate the k_p value as $k_p = k_g/(h\rho_{ox})^2$, 1.42×10^{-13} cm^2/s (or $\log k_p = -12.85$ cm^2/s). However, for 55 days and using the thickness of the grown oxide scale (3.5 μm), $k_p = 2.58 \times 10^{-14}$ cm^2/s (or $\log k_p = -13.59$ cm^2/s).

Sulfidation. TGA tests for sulfidation were conducted at 700°C in hydrogen that contained 500 ppm of H_2S. Figure 16 shows the equilibrium partial pressures of sulfur for Fe, Cr, and 500 ppm of H_2S/H_2, while Fig. 17 shows the sulfidized surface, scale cross section, and EDS spectrum for pure Cr.

Results of sulfidation of Fe-25Cr-1Ce with elemental maps (Fig. 18), and for Fe-25Cr-1Y (Fig. 19), showed heavy sulfide scales and separation from the alloy substrates. This indicates that the Y and Ce could not be considered as REEs in alloy sulfidation. However, in sulfidation tests on CVD-Fe-25Cr-0.3Y under the same conditions as for the above alloys, the sulfidation rate was significantly lower than that of the others (Fig. 20). When we consider the microstructure of the 55 days exposure sample, the specimen was relatively inert expect for some area that was sulfidized. X-ray examination showed that the surface scale was mainly Cr_3O_4 with some Cr_2O_3. We can say that alloy sulfidation may occur when the scale contains local reaction/diffusion channels (as seen in Fig. 21), which could not be blocked during the CVD process. However, in Fig. 22 (in another area along the cross section), we could not find any evidence reaction occurs with sulfur, so that the coating here can be considered ideal. Some sulfidation studies have been tried using Nb-implanted Fe-base alloys.[27,28] The implanted alloys exhibited substantially improved sulfur resistance. The CVD process in this study can be beneficial because it is technologically simple and relatively inexpensive. The smallest surface defects, grain boundaries, cracks, and fissures are modified to protect the entire surface of the alloy.

CONCLUSIONS

Reactive elements inhibit grain growth in the alloy: in decreasing order, alloy grain growth is as follows: Fe-25Cr >> Fe-25Cr-1Ce > Fe-25Cr-1Y. A durable protective coating for high-temperature alloys was achieved by CVD that was followed by chemical reaction in a controlled environment. Surface modification via a CVD process improves the protective properties. Without the benefit of an effective and long–lasting protective coating, the alloys are

attacked initially at microscopic surface defects, fissures, and microcracks, which are chemically active sites. The results of this study have elucidated the nature of the protective coating for high-temperature corrosion protection, namely, an extremely thin (1-2 μm) diffused silicon layer that covers the surface and penetrates even the smallest defects, cracks, etc., on the alloy to be protected. This method seems to offer great benefits for fabrication of heat-resistant alloys.

ACKNOWLEDGMENTS

This work was supported by the U.S. Department of Energy, under Contract W-31-109-Eng-38.

REFERENCES

1. Pfeil, L. B., Brit. Pat. No. 459,848 (1937).

2. "International Workshop on "Critical Issues Concerning the Mechanisms of High-Temperature Corrosion," Oxid. Metal **23** (5/6) (1985) 251-337.

3. "Oxidation of metals and associated mass transport," M. A. Dayananda, S. J. Rothman, and W. E. King, eds., Publ. Metallurgical Soc. (1987).

4. "Materials Science Forum,", Vol. 43 W. E. King, ed. (1989).

5. P. Kofstad, "High Temperature Corrosion," Elsvier Applied Science, New York (1988).

6. J. Oudar, in High Temperature Corrosion, R. A. Rapp, ed., NACE, Houston, TX, (1983) p 8.

7. J.-H. Park, "Surface Modification of High-Temperature Alloys: A protective and Scale Forming Process", presented at Electrochem. Soc. Meeting, Toronto, Oct. 11-16, extended abstract #508 (1992).

8. M. J. Graham, J. I. Eldride, D. F. Mitchel, and R. J. Hussey, Anion Transport in Growing Cr_2O_3 and Al_2O_3 Scales, Ref 3. pp. 207-242.

9. R. T. P. Whipple, Philos. Mag. 45 (1954) 1225.

10. T. Suzuoka, Trans. Japan Inst. Metals 2 (1961) 25.

11. A. D. LeClaire, Br. J. Appl. Phys., 14 (1963) 351-356.

12. A. Atkinson and R. I. Taylor, Philos. Mag. A, 43 (1981) 979-998.

13. J.-H. Park, W. E. King, and S. J. Rothman, J. Am. Ceram. Soc., 70 (1987) 880, and in Ref 3 pp. 103-107.

14. K. P. Lilerud and P. Kofstad, Oxid. Metal 17(1/2) (1982) 127-139.

15. A. G. Evans and T. G. Langdon, Prog. Mater. Sci., 21 177 (1976).

16. J.-H. Park and K. Natesan, Oxidation Behavior of Iron-Chromium Alloys at Elevated Temperatures: A Reactive-element Effect, Argonne National Laboratory Report ANL FE 92/1 (1992)

17. J.-H. Park, Mat. Lett. 8(10) (1989) 405-408.

18. W. E. King and J.-H. Park, Coll. de Phy. 51, C1-551(1990) and Proc. 1988 Spring Meeting of Mater. Res. Soc., 122 Materials Research Society, Pittsburgh (1989) 193.

19. R. A. Rapp, Metall. Trans., 15A (1984) 765.

20. J.-H. Park and K. Natesan "Alloy Grain Growth in High-Temperature Oxidation," presented at Electrochem. Soc. Meeting, Phoenix, AZ, Oct. 13-17, extended abstract #620 (1991).

21. King, W. E., N. L Peterson, and J. F. Reddy, J. Physique, 46, C4-423 (1985).

22. C. M. Cotell, G. J. Yurek, R. J. Hussey, D. F. Mitchell, and M. J. Graham, Oxid. Metal **34**(3/4) (1990) 173-200, and 201-216.

23. R. P. Elliott, "Constitution of Binary Alloys, First Supplement," McGraw-Hill Book Co., New York (1965).

24. M. Hansen, "Constitution of Binary Alloys," McGraw-Hill Book Co., New York (1958).

25. D. Shore, Univ. Minnesota, personal communication (1992)

26. M. Hillert, Acta Metall., **36** (12) (1988) 3177-3181.

27. K. Natesan and J.-H. Park, "Role of Alloying Additions in the Oxidation-Sulfidation of Fe-Based Alloys" in "Corrosion & Particle Erosion at High-Temperatures," V. Srinivasan and K. Vedula, eds., Proc. Symp. TMS-ASM

Joint Corrosion and Environmental Effects Committee, 118th meeting TMS, Las Vegas, Nevada, Feb. 27-March 3 (1989) pp. 49-64.

28. J.-H. Park, Sulfidation on Nb-sputtered deposited Fe-based Alloys, unpublished results (1989).

Table 1. Comparison of IBAD and CVD processes.

	IBAD (Ion-Beam -Assisted Deposition)		CVD (Chemical Vapor Deposition)
	No Heat Treatment	After Heat Treatment	Annealing
XRD	Amorphous	Cr_2O_3 Fe-Cr-Silicides	Cr_2O_3 Fe-Cr-Silicides
Auger	———	Si, N, O	———
XPS	———	Si, N, O	———
SEM	Good Adhesion	Good Adhesion	Good Adhesion

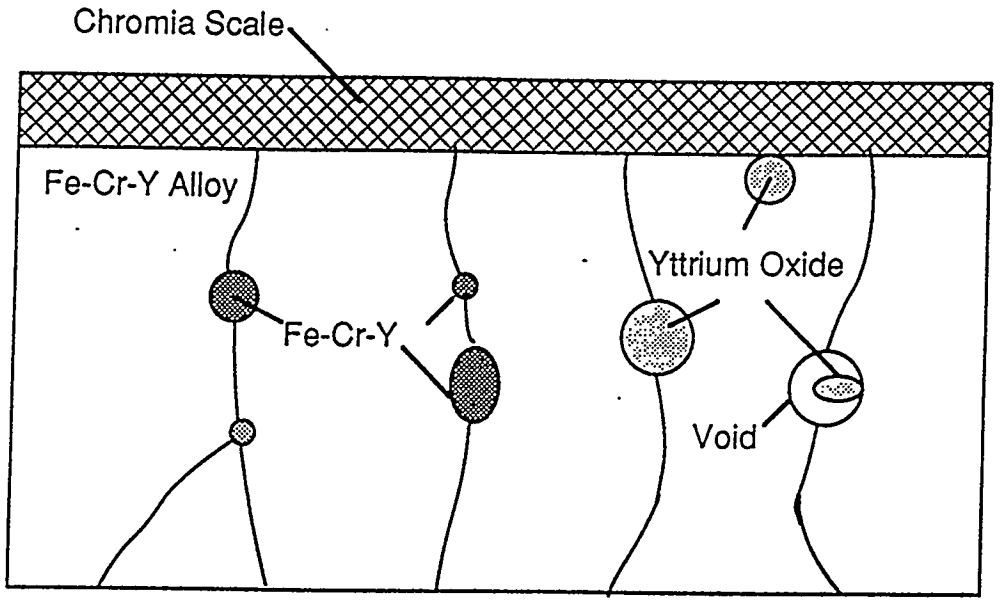

Fig. 1 Grain-growth inhibition by Fe-Cr-Y and Y_2O_3 segregated in alloy grain boundaries.

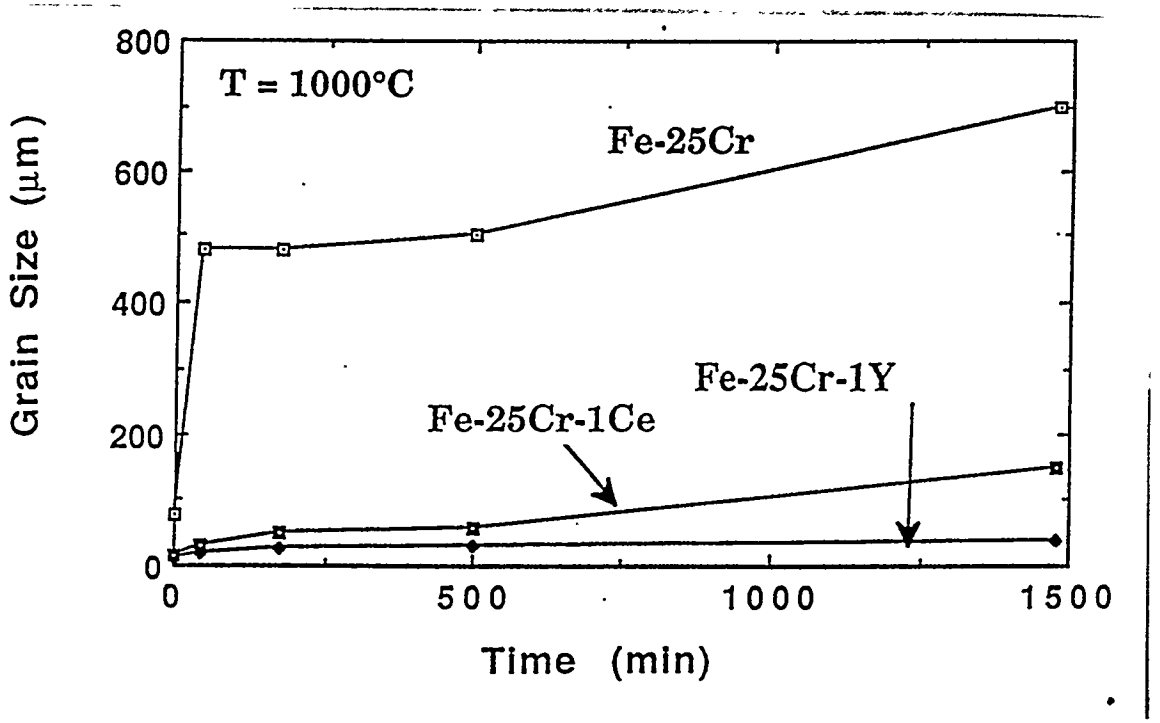

Fig. 2 Alloy grain growth for Fe-25Cr, Fe-25Cr-1Ce, and Fe-25Cr-1Y vs. time at 1000°C.

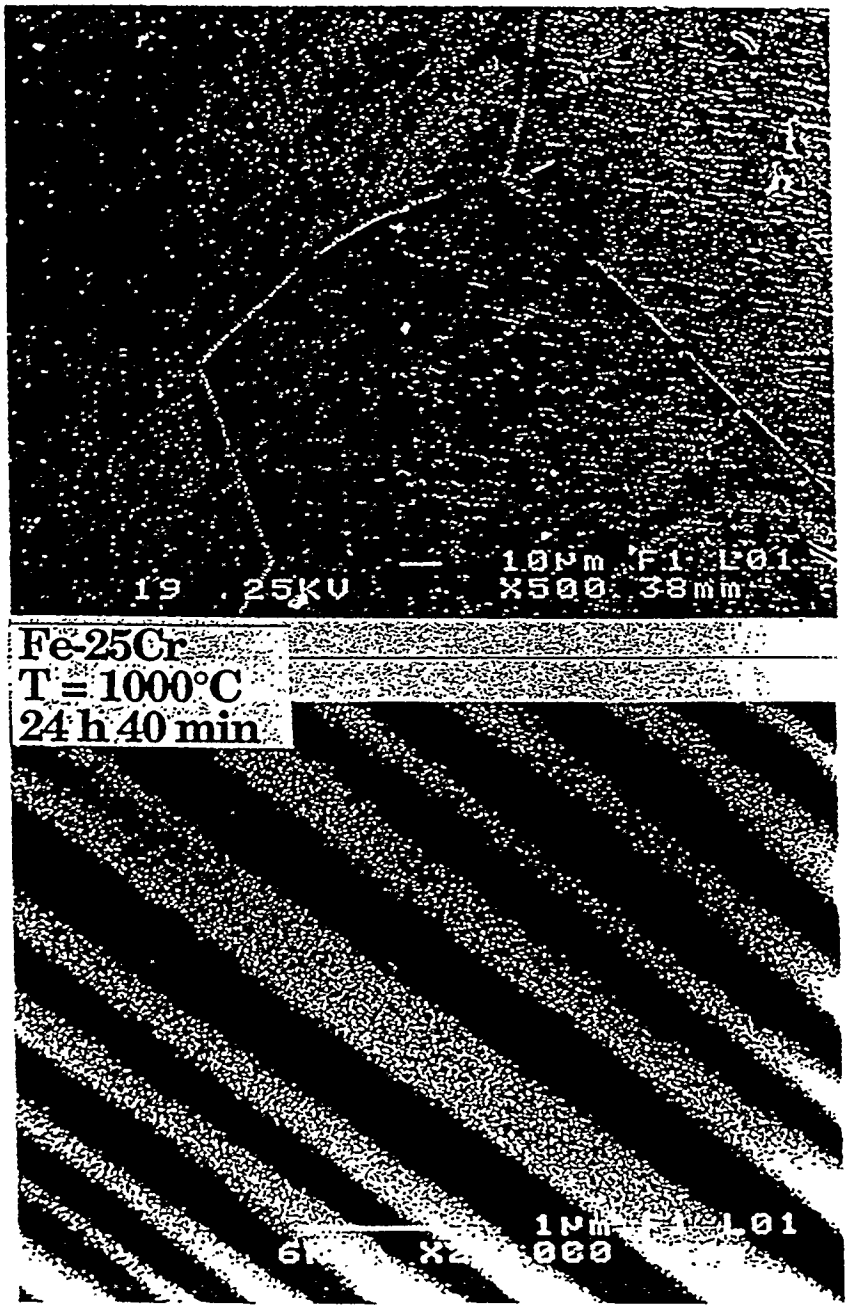

Fig. 3 Alloy surfaces of (a) Fe-25Cr, (b) Fe-25Cr-1Ce, and (c) Fe-25Cr-1Y at 1000°C for 24 h 40 min.

T:9-5a

fig-3b

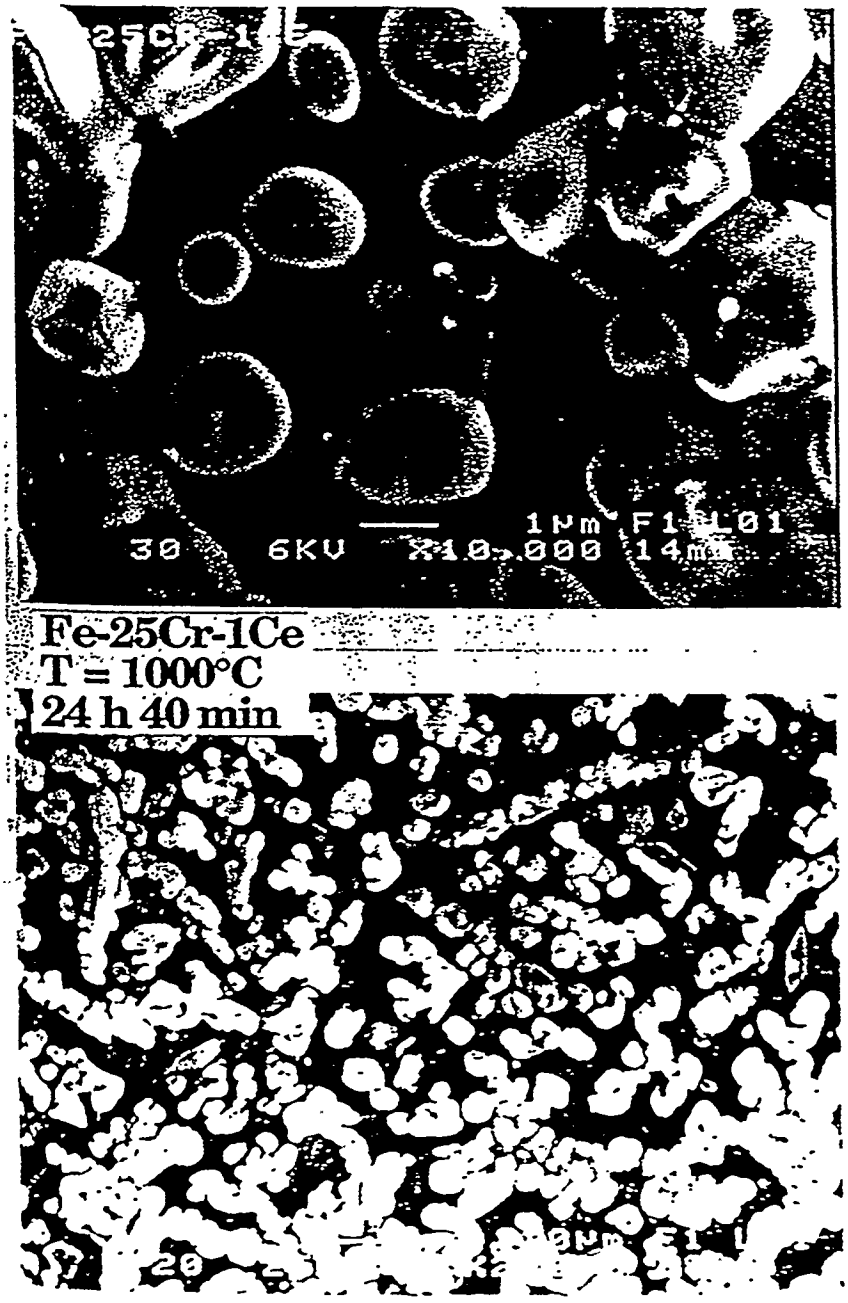

fig-3c

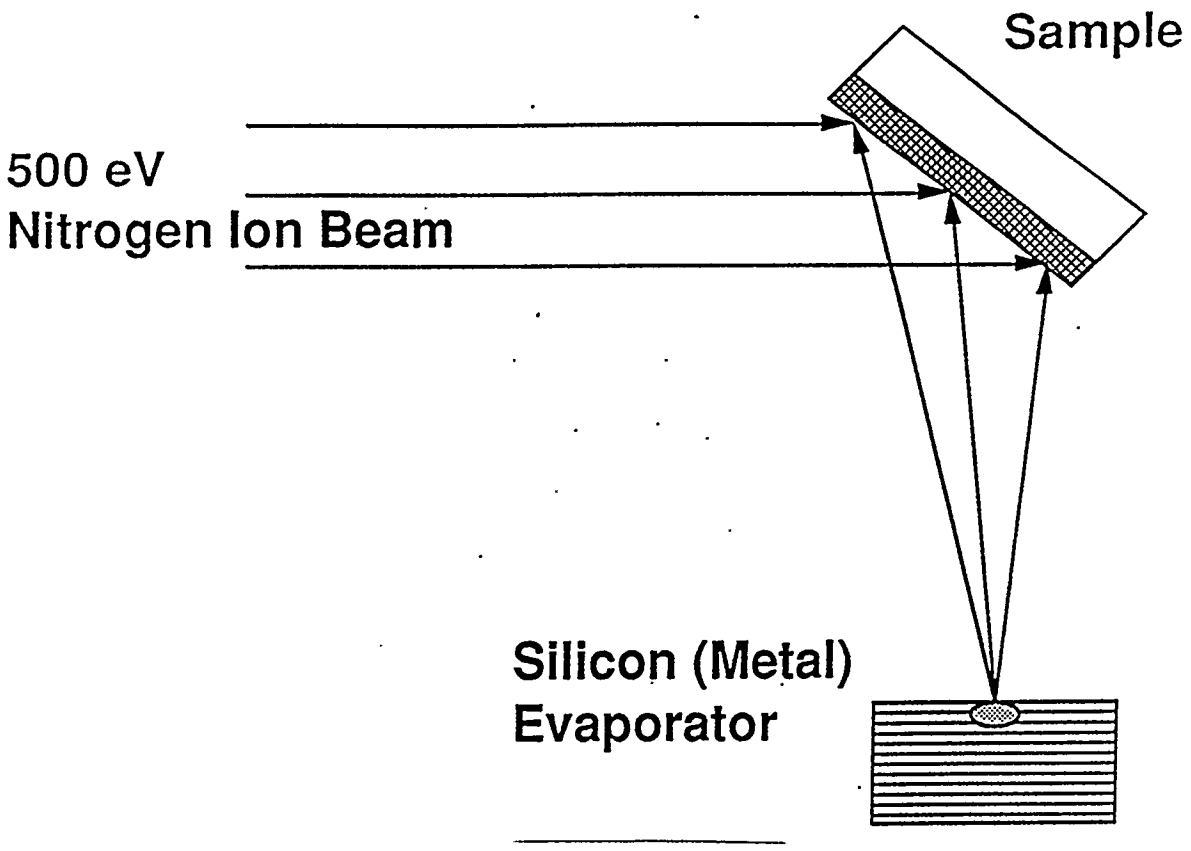

Fig. 4 Schematic diagram of IBAD apparatus.

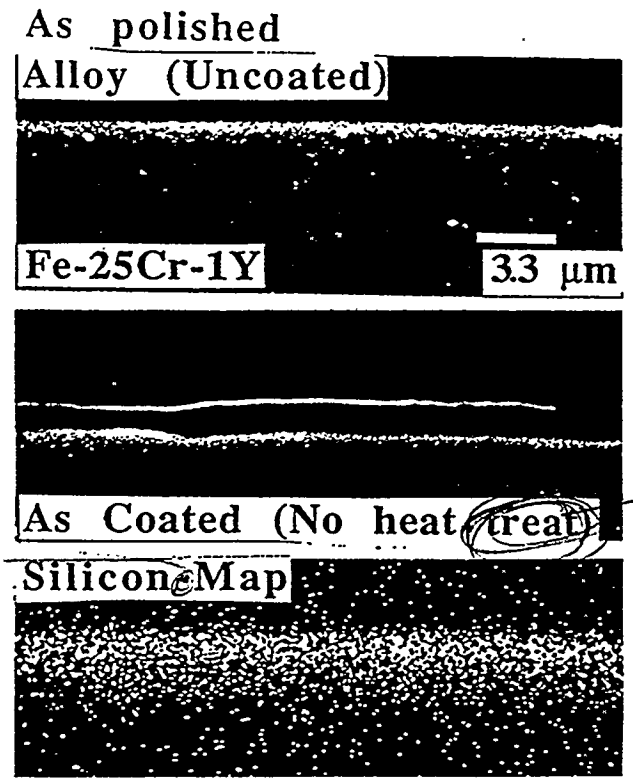

Fig. 5 (a) Cross section of uncoated and coated Fe-25Cr-0.3Y by IBAD and silicon map before heat treatment, and (b) cross section and surface of coated and uncoated Fe-25Cr-0.3Y by IBAD, silicon map, and EDS after heat treatment.

fig-5a

Fig-5b

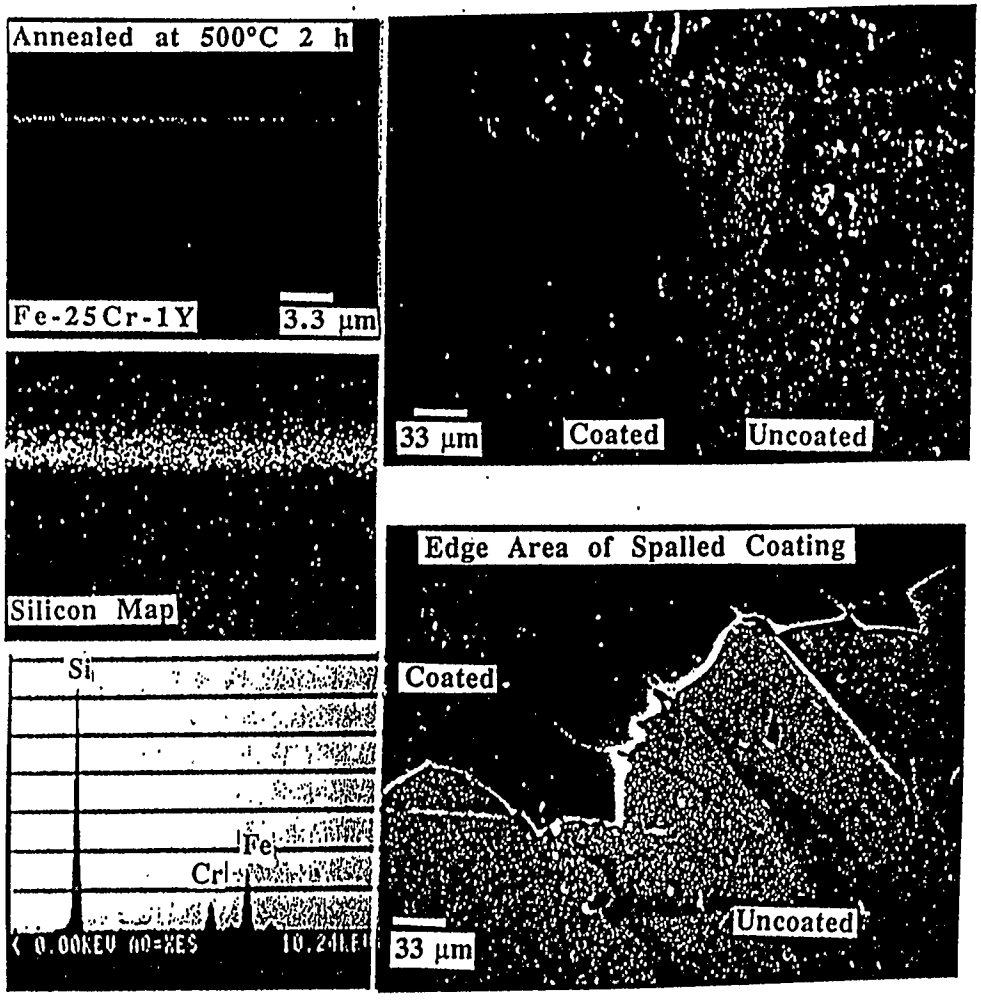
Annealed at 500°C 2 h
Fe-25Cr-1Y
3.3 µm
Silicon Map
Si
Fe
Cr
33 µm
Coated
Uncoated
Edge Area of Spalled Coating
Coated
Uncoated
33 µm

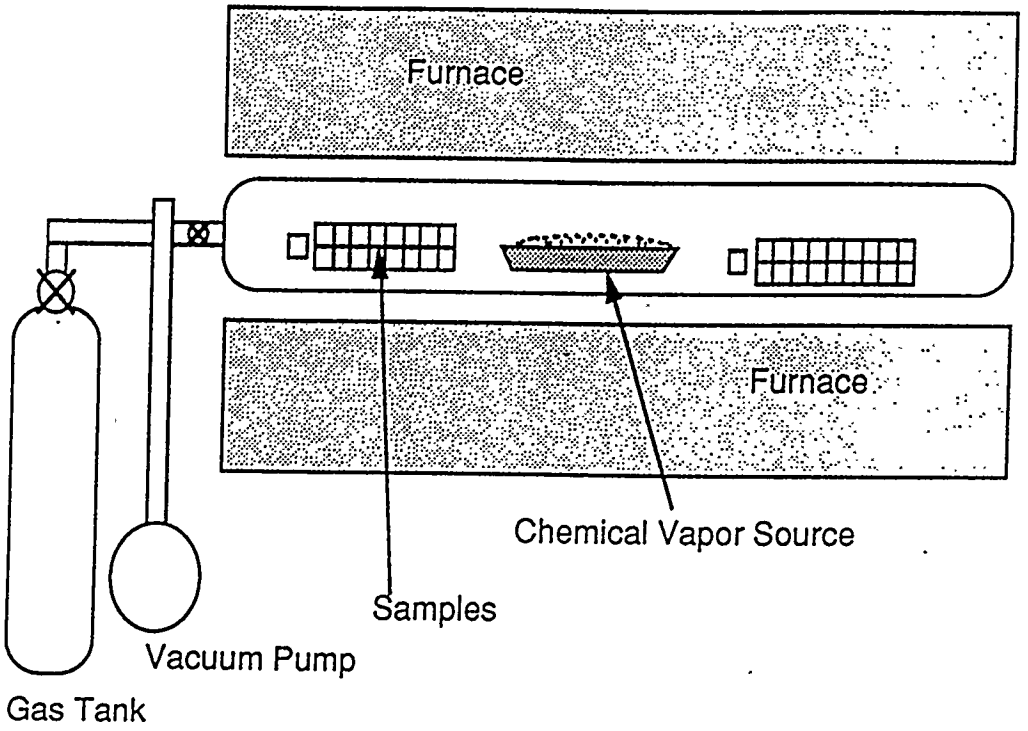

Fig. 6 Schematic diagram of CVD apparatus.

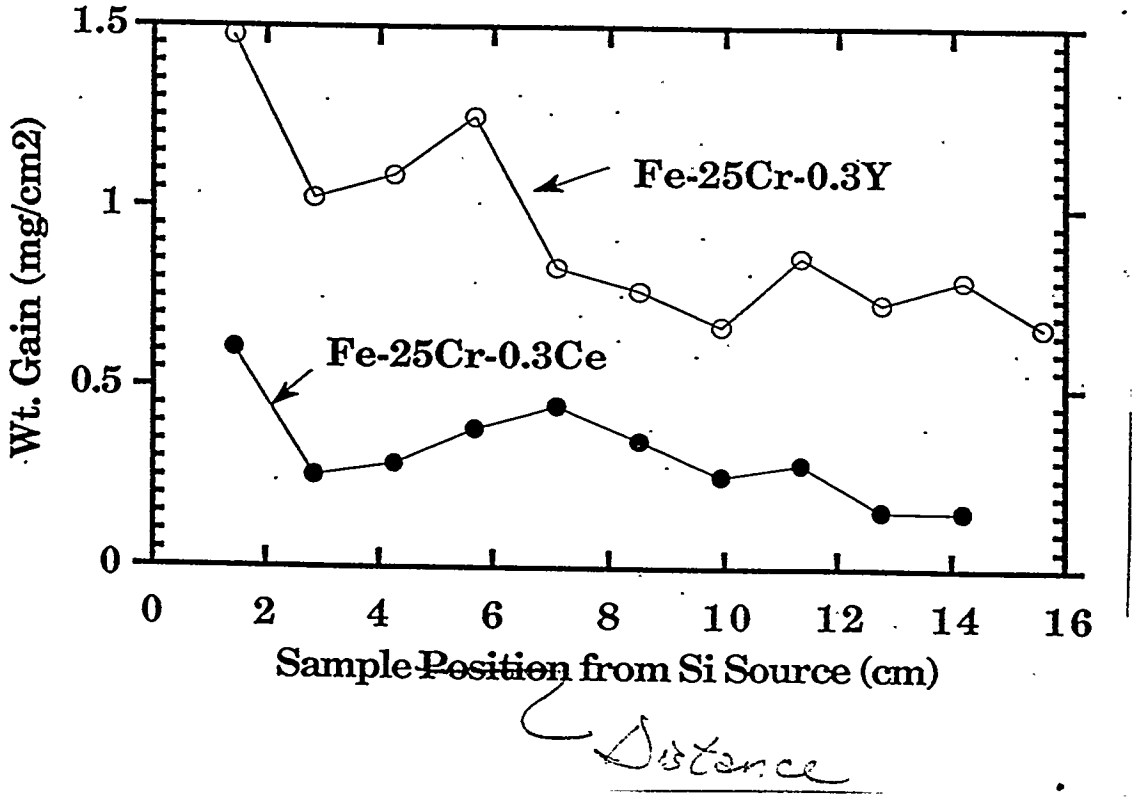

Fig. 7 Weight gain vs. specimen distance from Si source for Fe-25Cr-0.3 Ce and Fe-25Cr-0.3Y.

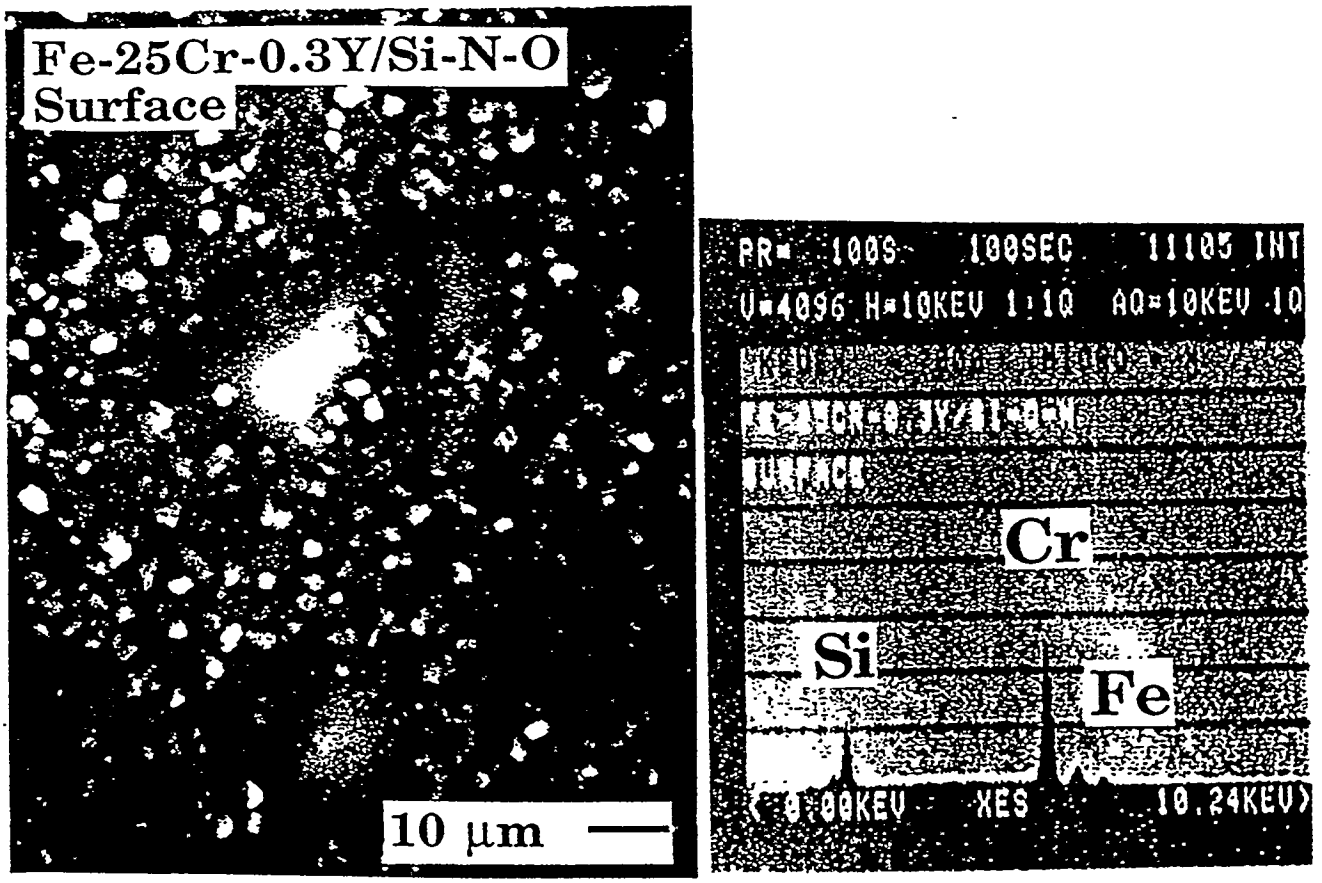

Fig. 8 CVD coating surfaces and EDS for (a) Fe-25Cr-0.3Y and (b) Fe-25Cr-0.3Ce.

fig-8a

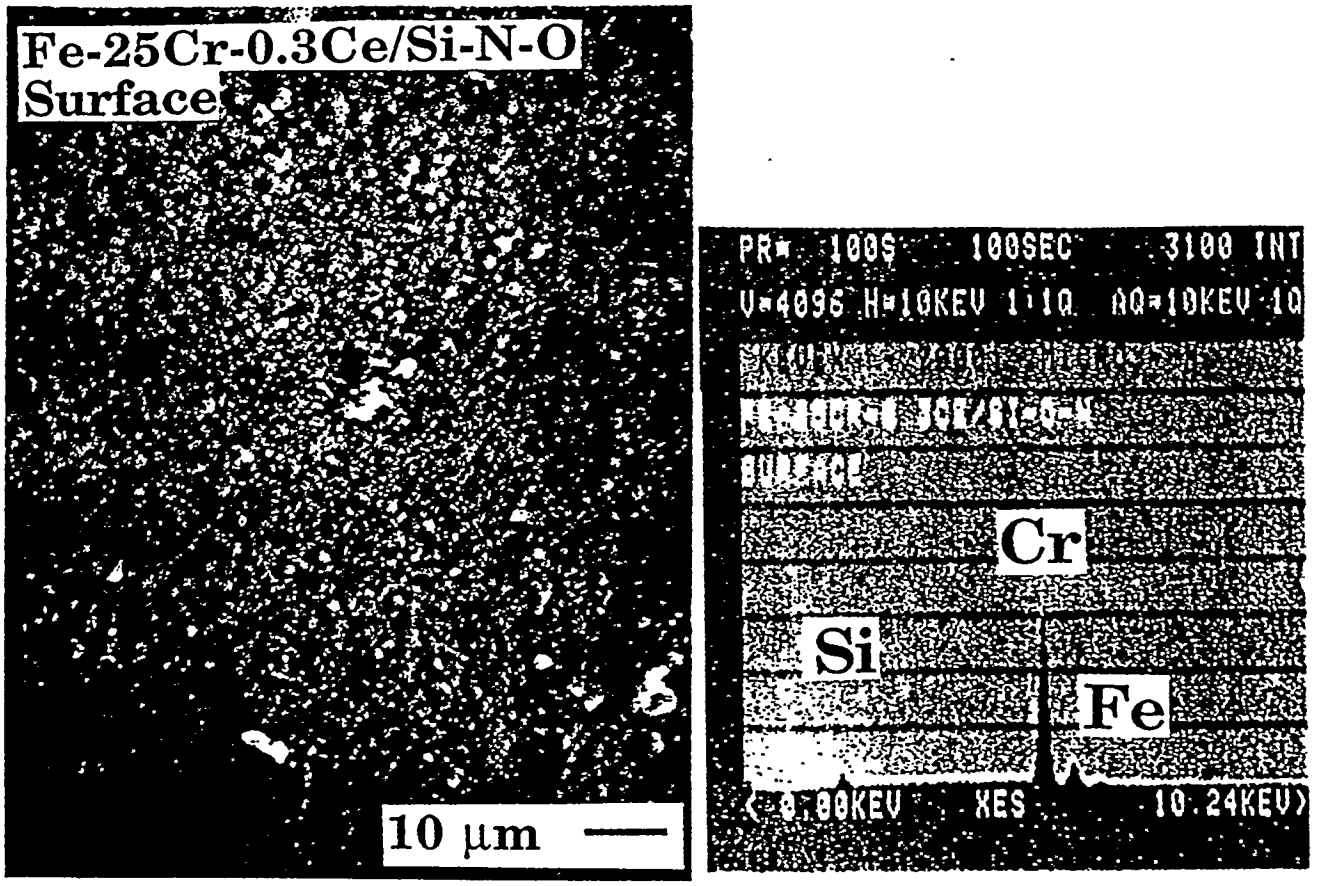
Fe-25Cr-0.3Ce/Si-N-O
Surface
10 μm
PR= 100S 100SEC 3100 INT
V=4096 H=10KEV 1:10 AQ=10KEV 10
Cr
Si
Fe
0.00KEV XES 10.24KEV

fig-8b

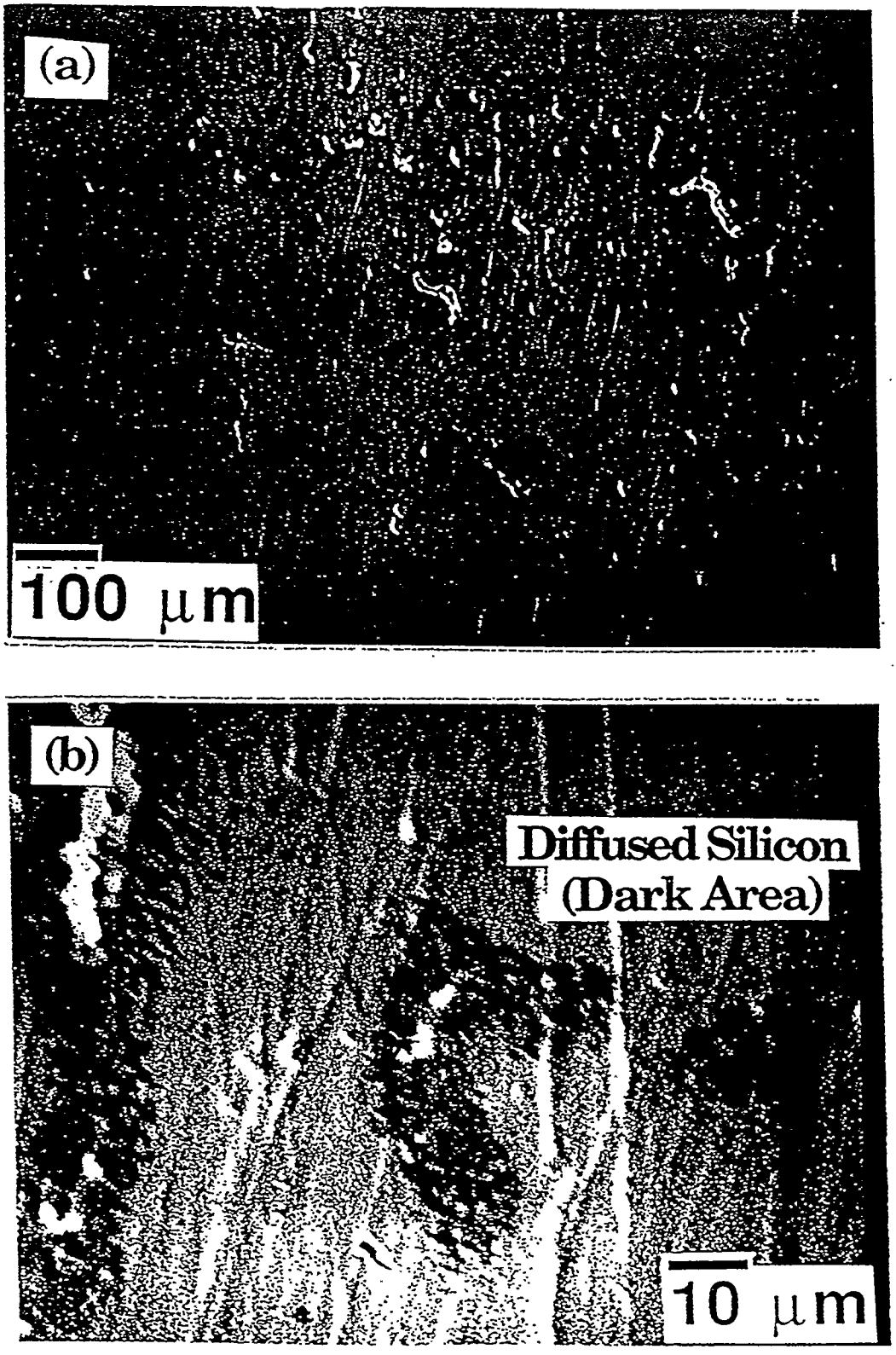

Fig. 9 (a) Silicon diffusion (darker gray areas) into and around the surface (surface silicon was removed), and (b) enlargement of area at right center of (a) for Fe-25Cr-0.3Y.

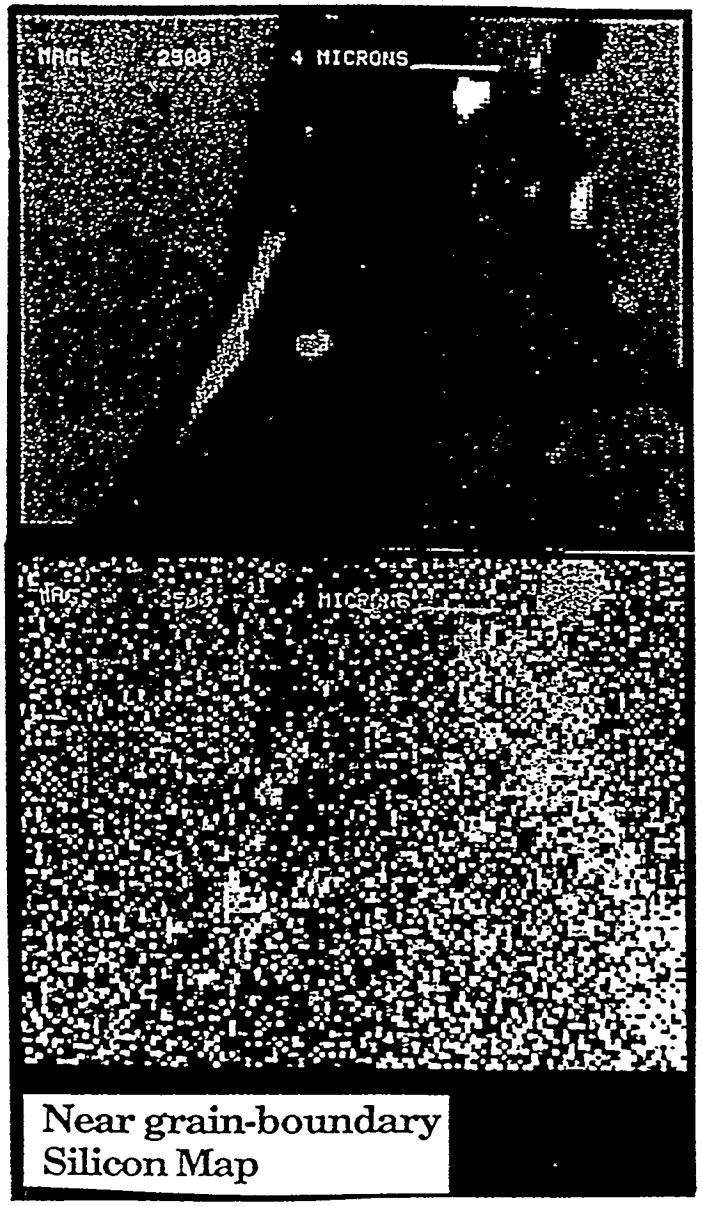

Fig. 10 TEM and silicon mapping near alloy grain boundary (right bottom).

fig-10

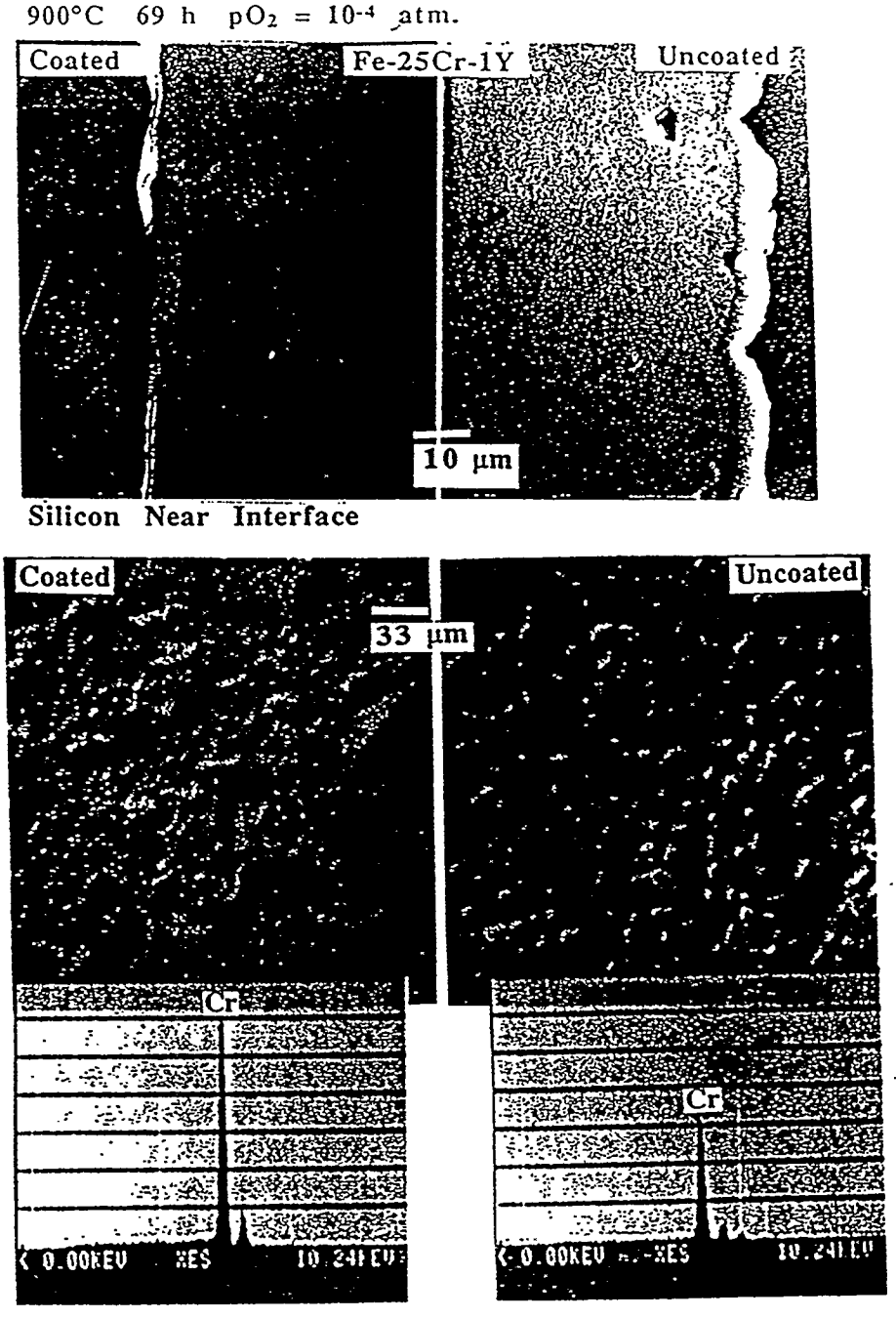

Fig. 11 Interface of alloy/scale and surface of coated and uncoated Fe-25Cr-0.3Y by IBAD, of oxidized at 900°C for 69 h in $pO_2 = 10^{-4}$ atm. Shown at bottom are EDS results for each surface.

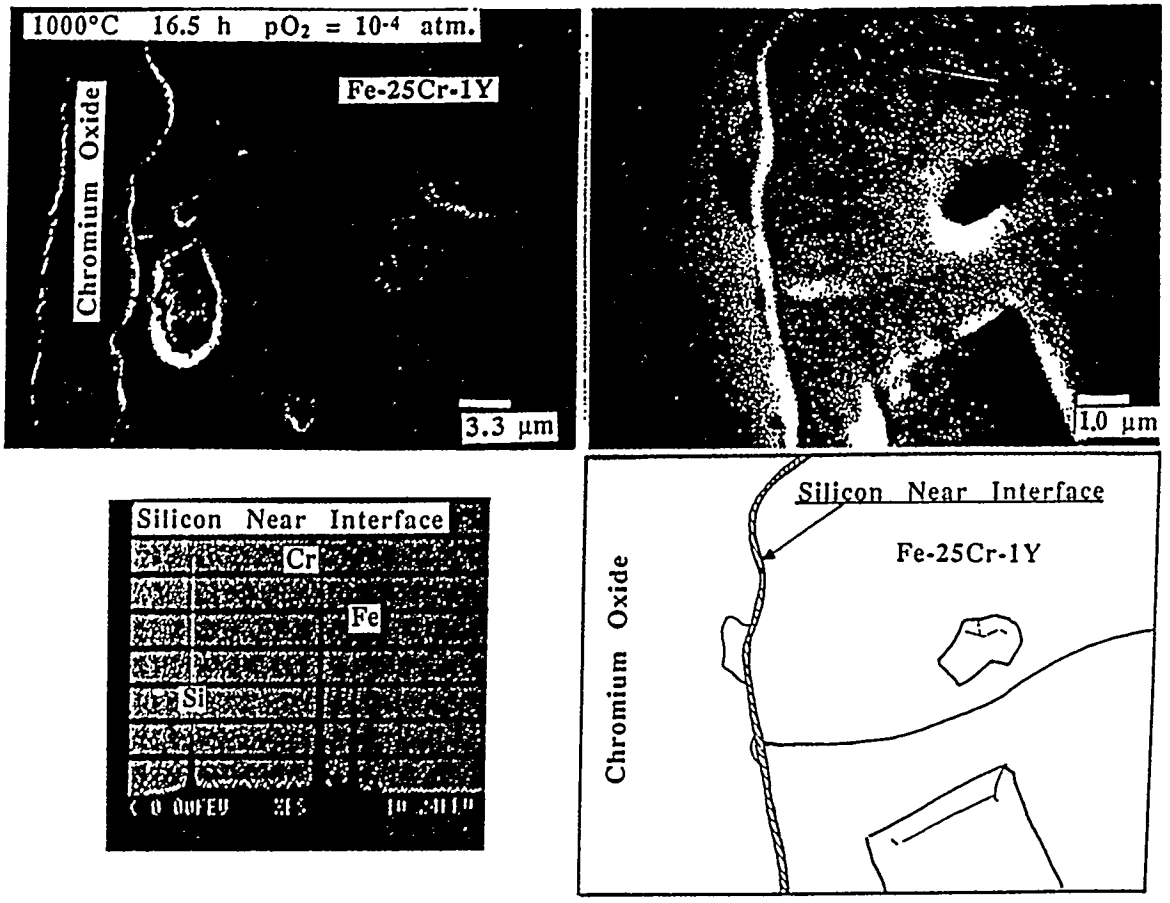

Fig. 12 Interface of alloy/scale-coated Fe-25Cr-0.3Y by IBAD; oxidized at 1000°C for 16.5 h in $pO_2 = 10^{-4}$ atm. Diagram at lower right shows position of silicon.

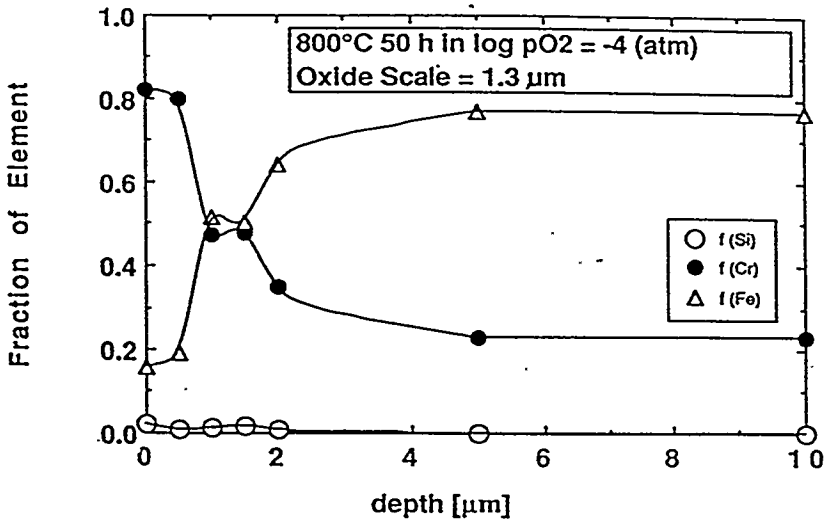

(a)

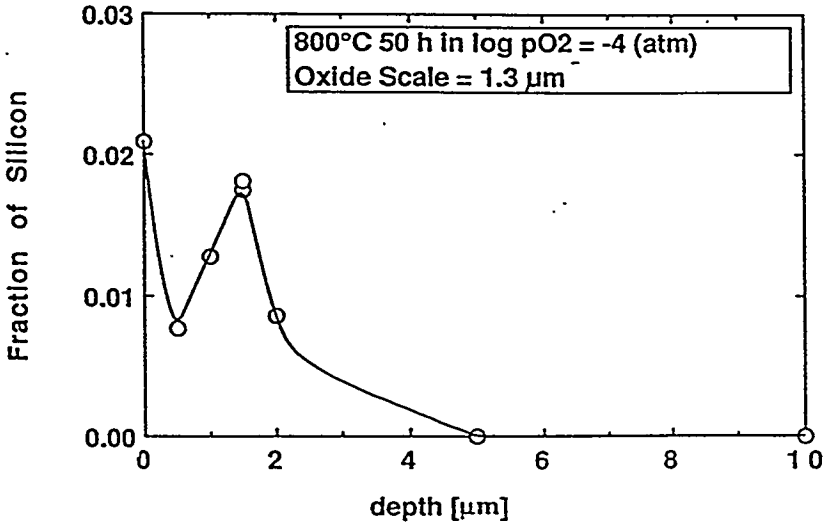

(b)

Fig. 13 (a) Depth profile for interface of alloy/scale-coated Fe-25Cr-0.3Y by IBAD; oxidized at 800°C for 50 h in $pO_2 = 10^{-4}$ atm; (b) detailed silicon profile.

Fig-13

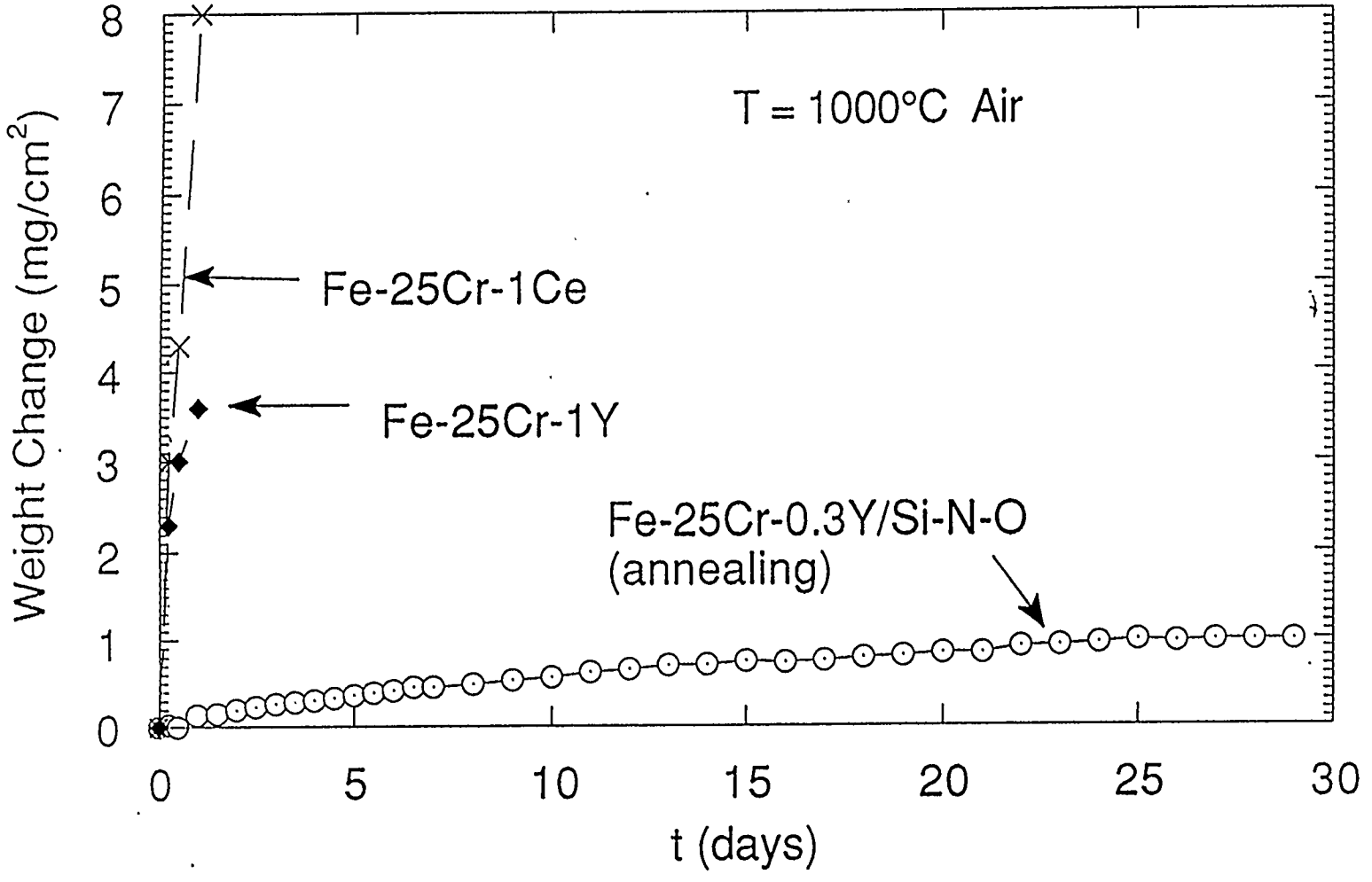

Fig. 14. Weight change vs. time for oxidation of CVD-Fe-25Cr-0.3Y, Fe-25Cr-1Ce, and Fe-25Cr-1Y at 1000°C in air.

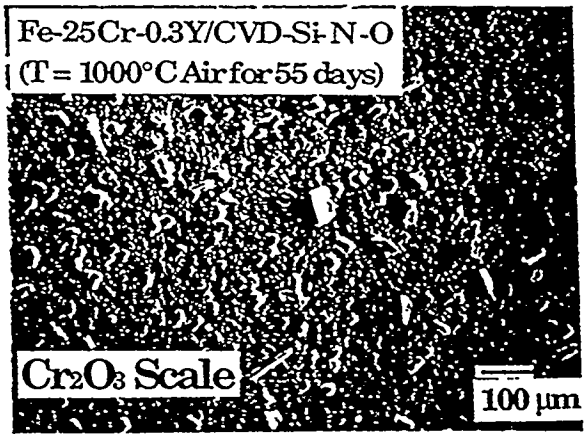

(a)

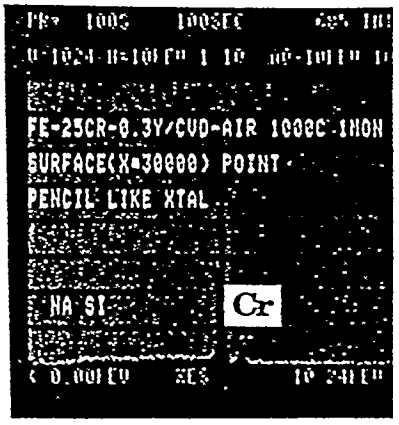

(b)

Fig. 15. (a) Surface of CVD alloy Fe-25Cr-0.3Y oxidized at 1000°C for 55 days, and (b) EDS results.

f:9-15

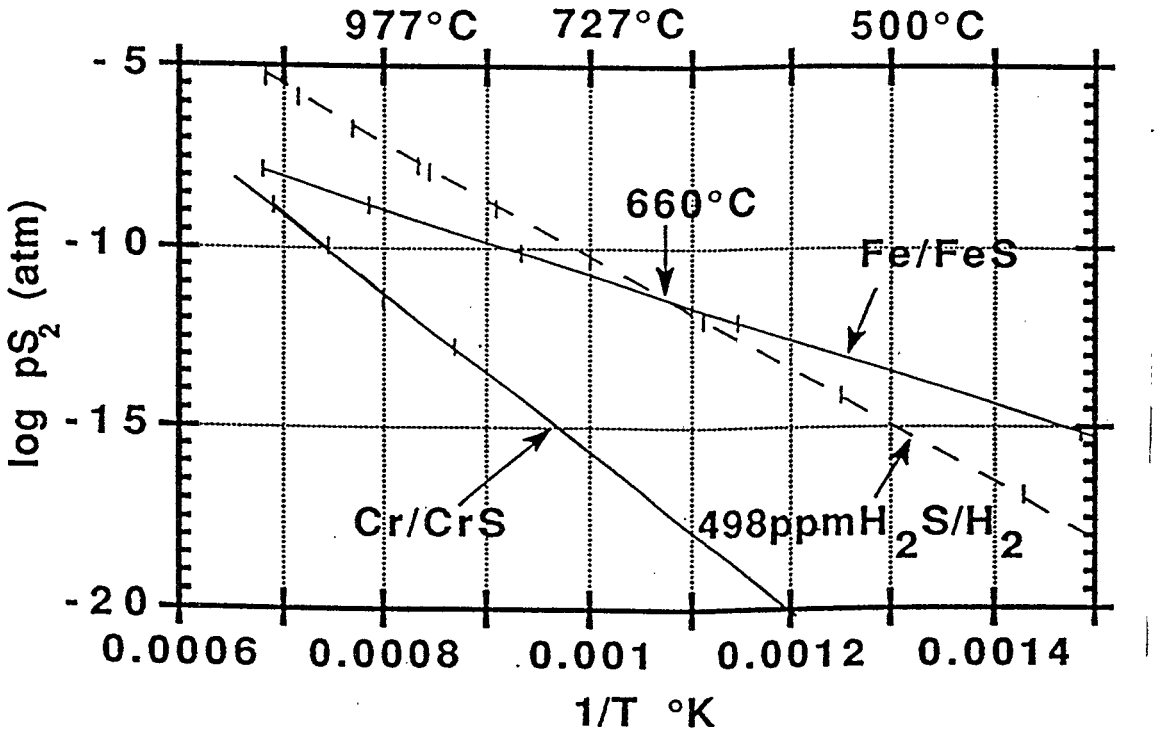

Fig. 16. Log pS_2 vs. 1/T for 498 ppm H_2S/H_2, Cr/CrS, and Fe/FeS.

fig-17

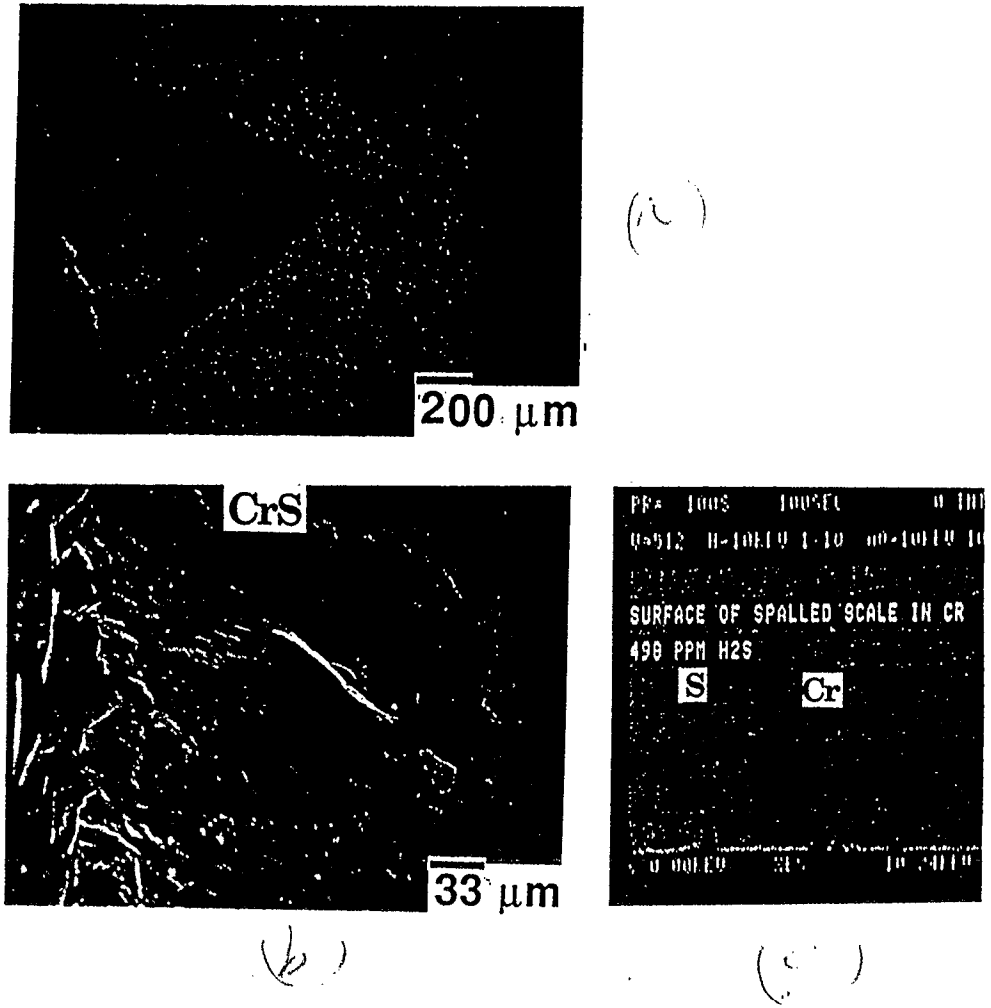

Fig. 17. (a) Sulfidation of pure Cr at 700°C for 120 h at surface, (b) scale cross-section, and (c) EDS results.

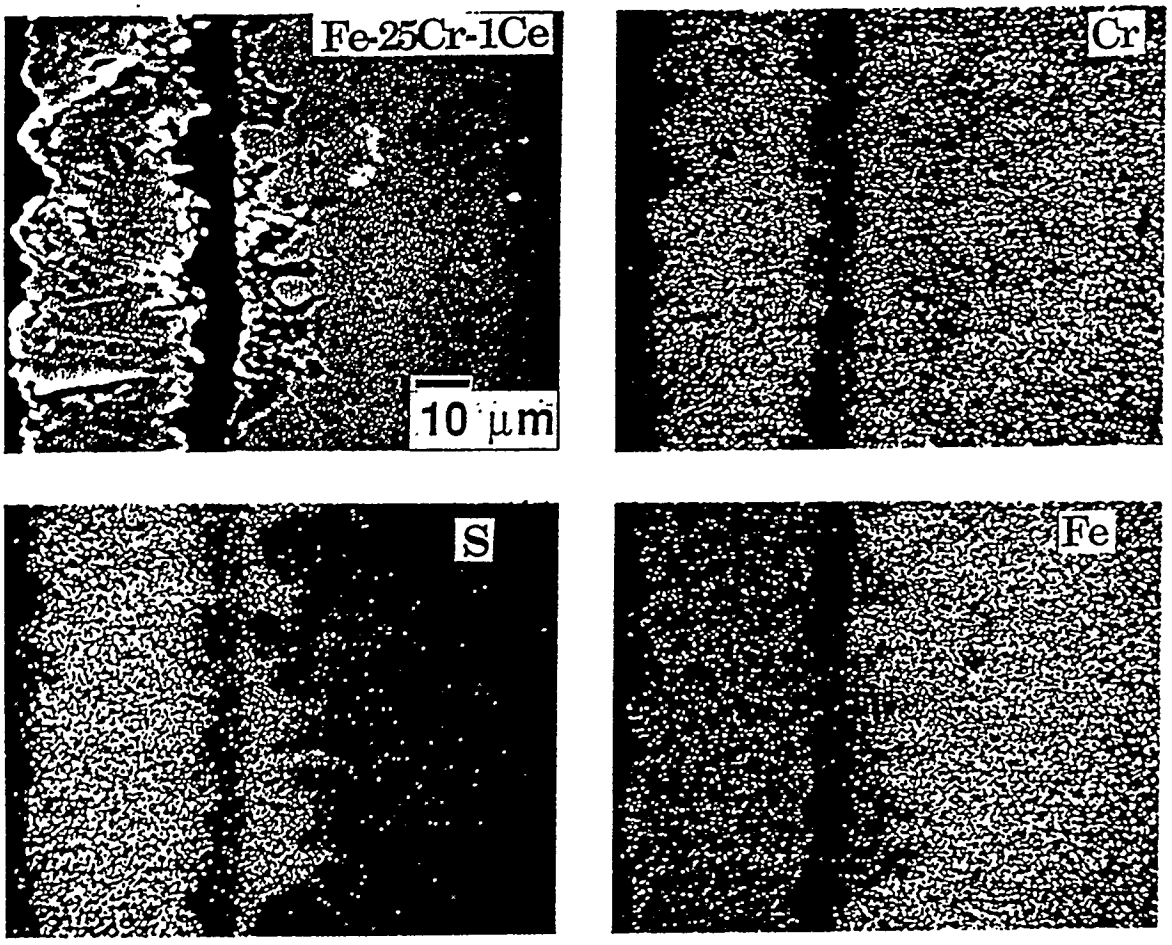

Fig. 18. (a) Cross section and elements map for sulfidation of Fe-25Cr-1Ce at 700°C for 72 h at the surface, (b) scale cross-section and (c) EDS results.

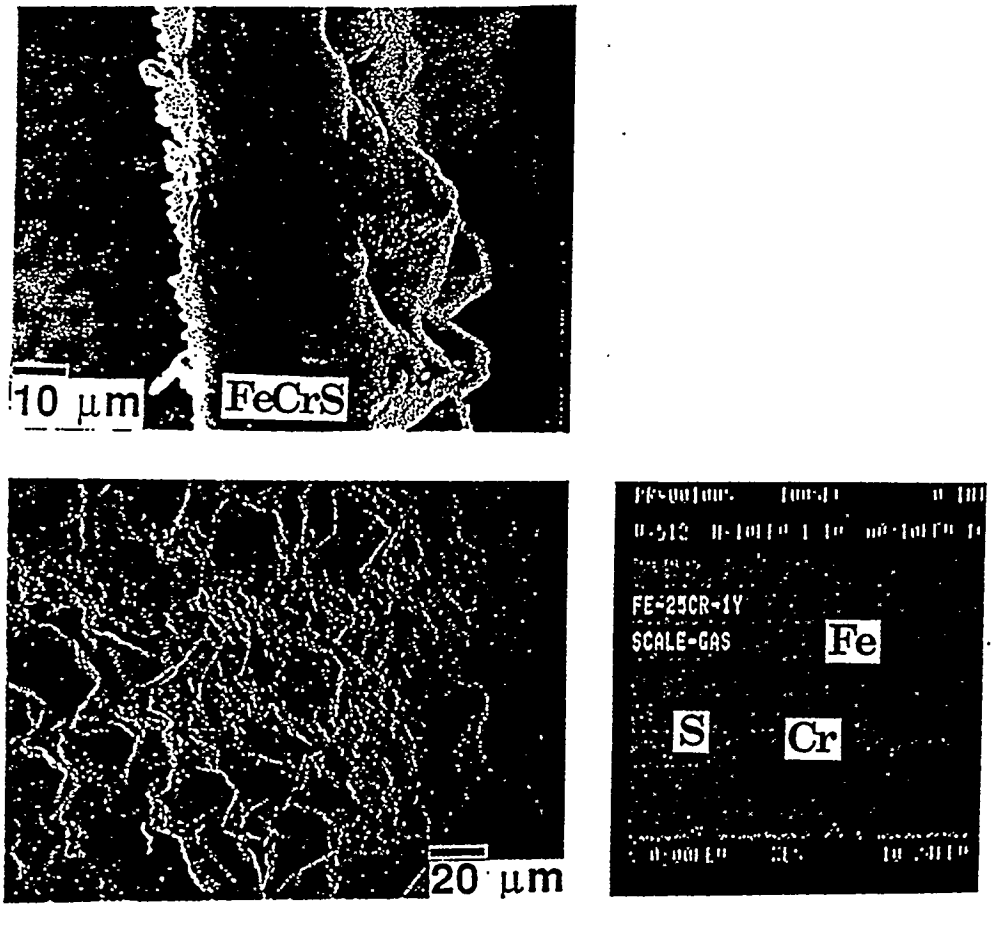

Fig. 19. (a) Cross section and the surface for sulfidation of Fe-25Cr-1Y at 700°C for 72 h at the surface, (b) scale cross-section, and (c) EDS results.

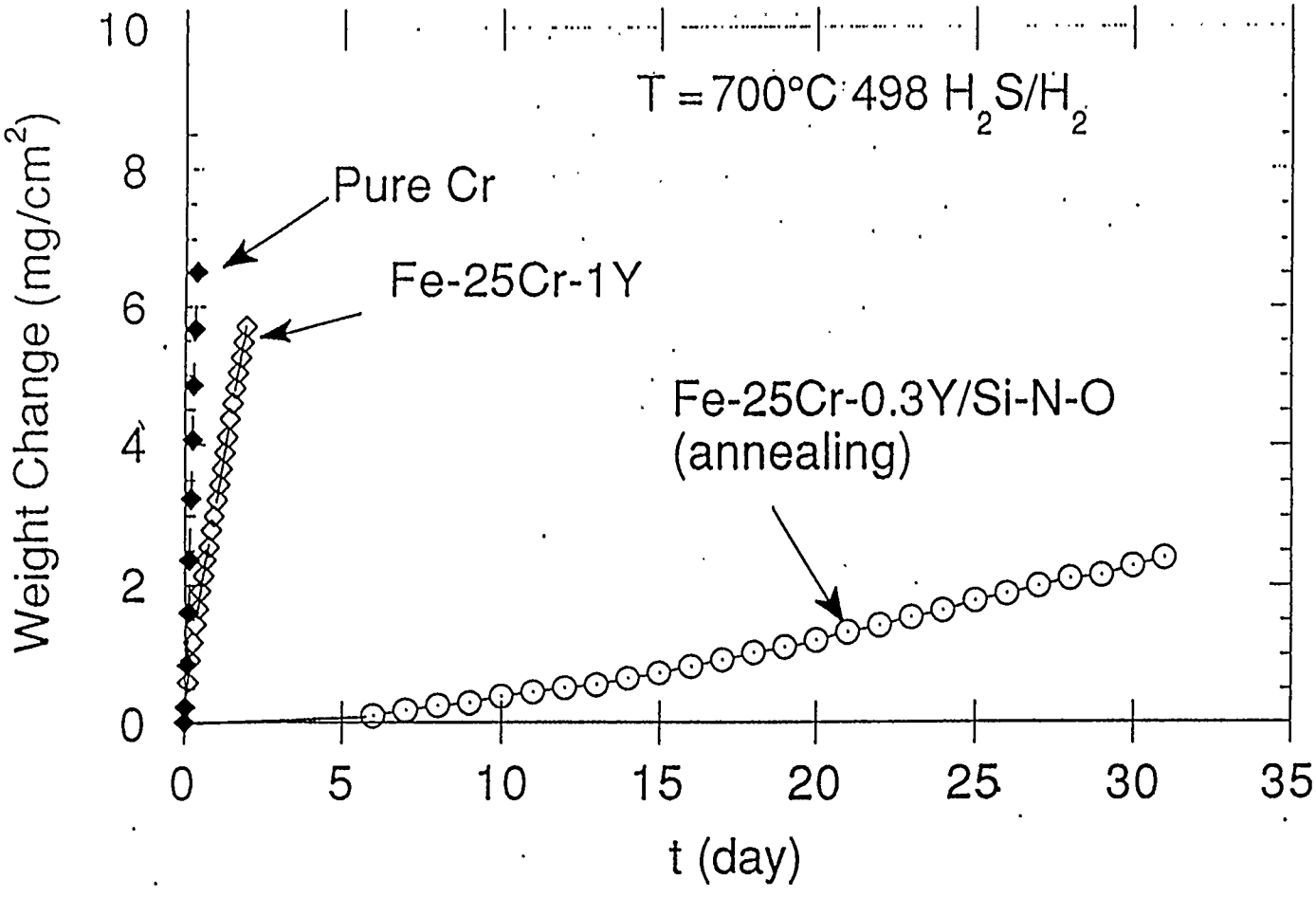

Fig. 20. Weight change vs. time for sulfidation of CVD-Fe-25Cr-0.3Y, pure Cr, and Fe-25Cr-1Y at 700°C in 498 ppm H_2S/H_2.

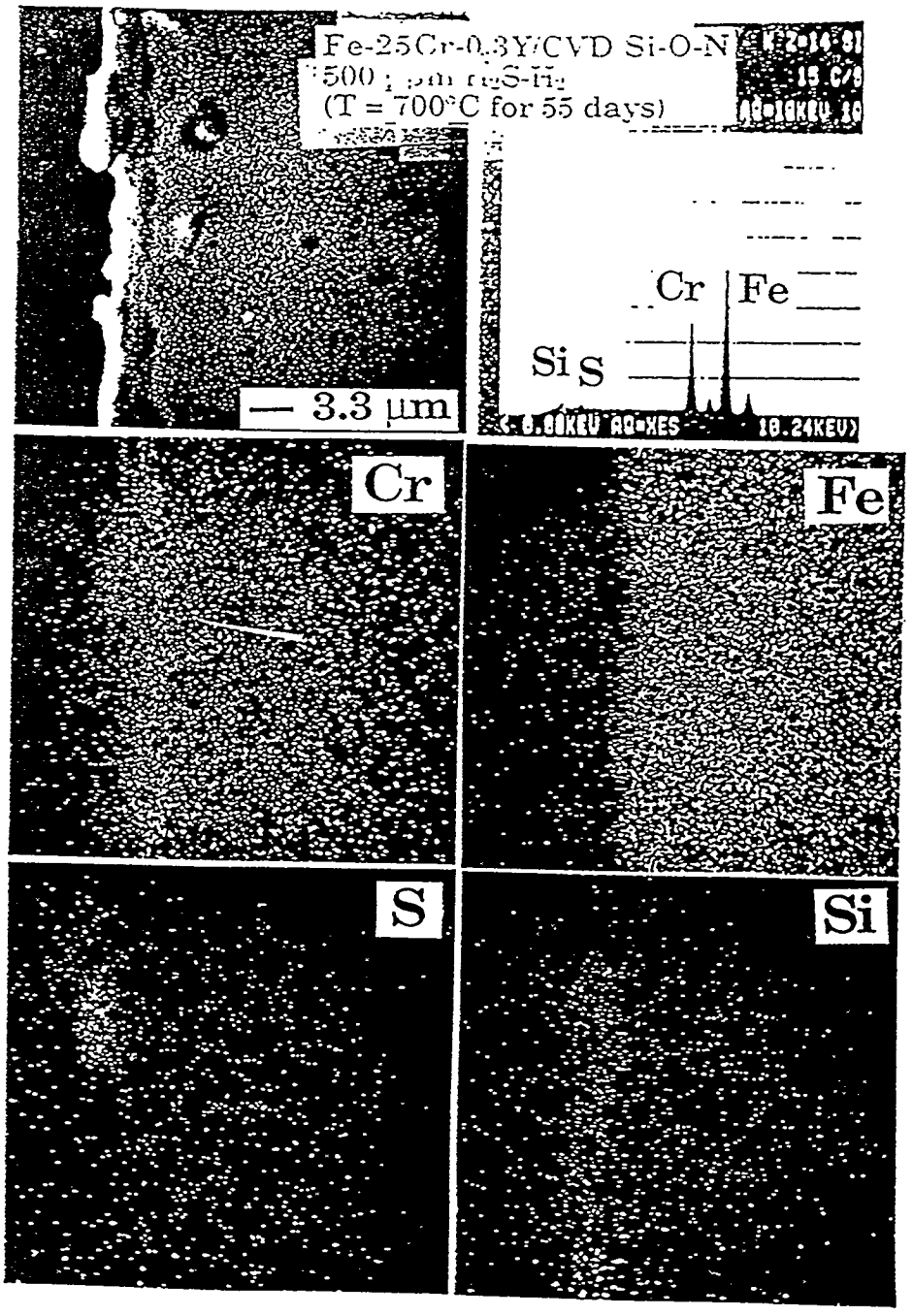

Fig. 21. Cross-section of CVD Fe-25Cr-0.3Y after sulfidation at 700°C for 55 days; with EDS and element maps.

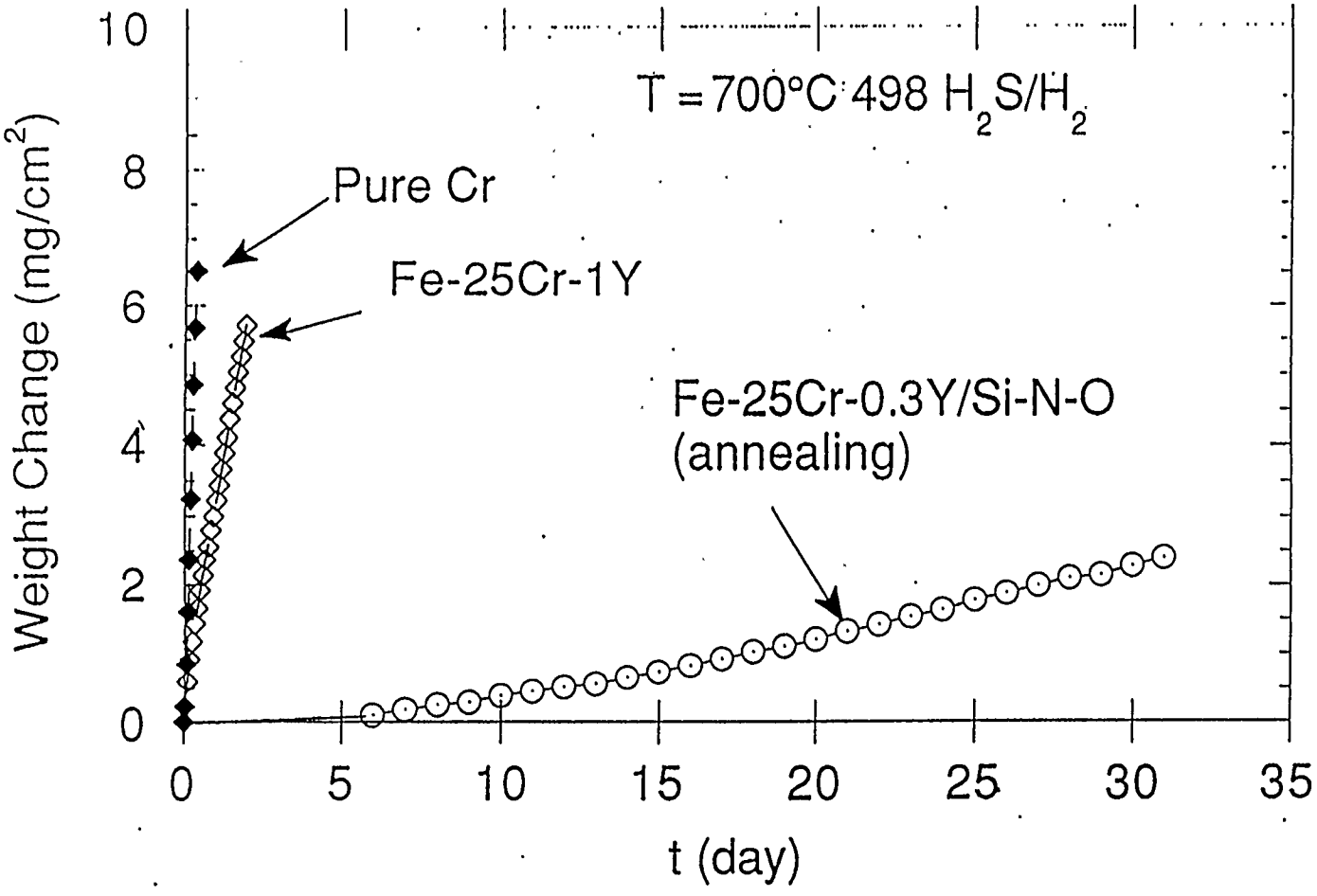

Fig. 20. Weight change vs. time for sulfidation of CVD-Fe-25Cr-0.3Y, pure Cr, and Fe-25Cr-1Y at 700°C in 498 ppm H_2S/H_2.

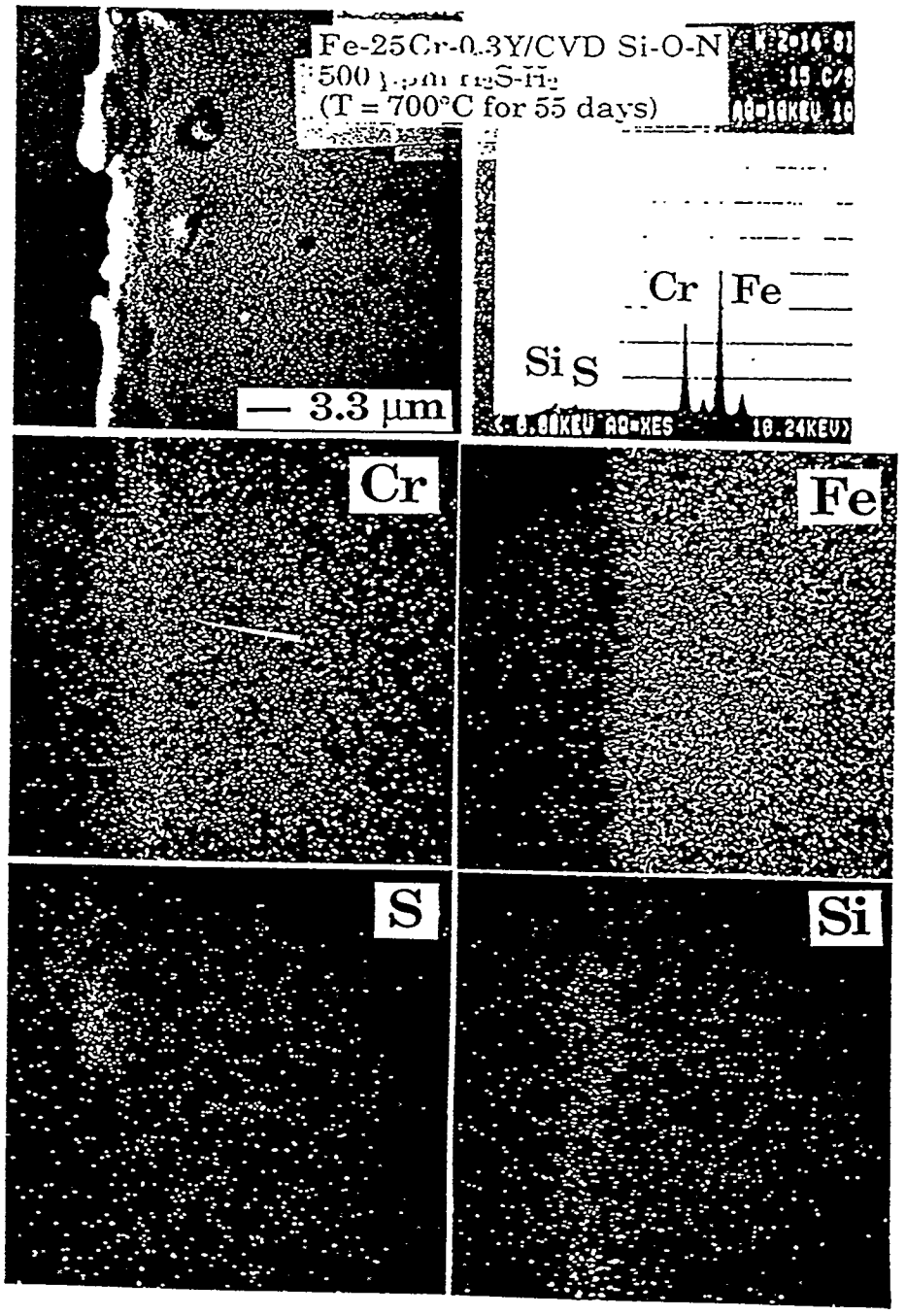

Fig. 21. Cross-section of CVD Fe-25Cr-0.3Y after sulfidation at 700°C for 55 days; with EDS and element maps.

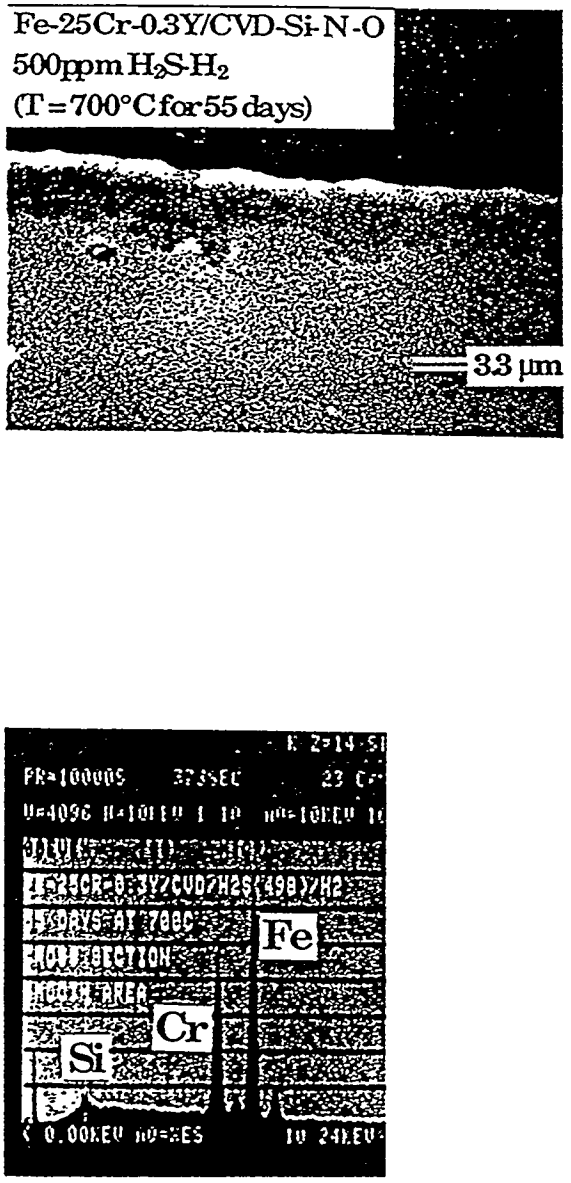

Fig. 22. Corrosion resistance of coated alloy Fe-25Cr-0.3Y/Si-N-O in a sulfur-containing atmosphere. No sulfur was detected in this area.